Table S1. New species introduced in AERO7 compared to AERO6. Species 1-21 are new to AERO7i. Other species in AERO7i (including species 22-24) previously existed in AERO6i. All gas-phase semi-volatiles use species-specific wet and dry deposition surrogates. Note that underscores are no longer used in species names in any aerosol or non-reactives namelist. For example, SV_ISO1 is now SVISO1 in the non-reactives namelist (i.e. NR*.nml) in CMAQ.

	Species	Phase	Description	Scientific Basis	Model Implementation
1	AMT1J	particle	low volatility particulate matter from monoterpene photoxidation (OH and O_3 reaction), C*=0.01 μg m^{-3}	dark α-pinene ozonolysis (Saha and Grieshop, 2016, *ES&T*)	Xu et al., 2018, *ACP*
2	AMT2J	particle	low volatility particulate matter from monoterpene photoxidation (OH and O_3 reaction), C*=0.1 μg m^{-3}	dark α-pinene ozonolysis (Saha and Grieshop, 2016, *ES&T*)	Xu et al., 2018, *ACP*
3	AMT3J	particle	semivolatile particulate matter from monoterpene photoxidation (OH and O_3 reaction), C*=1 μg m^{-3}	dark α-pinene ozonolysis (Saha and Grieshop, 2016, *ES&T*)	Xu et al., 2018, *ACP*
4	AMT4J	particle	semivolatile particulate matter from monoterpene photoxidation (OH and O_3 reaction), C*=10 μg m^{-3}	dark α-pinene ozonolysis (Saha and Grieshop, 2016, *ES&T*)	Xu et al., 2018, *ACP*
5	AMT5J	particle	semivolatile particulate matter from monoterpene photoxidation (OH and O_3 reaction), C*=100 μg m^{-3}	dark α-pinene ozonolysis (Saha and Grieshop, 2016, *ES&T*)	Xu et al., 2018, *ACP*
6	AMT6J	particle	semivolatile particulate matter from monoterpene photoxidation (OH and O_3 reaction), C*=1000 μg m^{-3}	dark α-pinene ozonolysis (Saha and Grieshop, 2016, *ES&T*)	Xu et al., 2018, *ACP*
7	SVMT1	gas	low volatility gas from monoterpene photoxidation (OH and O_3 reaction), C*=0.01 μg m^{-3}	dark α-pinene ozonolysis (Saha and Grieshop, 2016, *ES&T*)	Xu et al., 2018, *ACP*
8	SVMT2	gas	low volatility gas from monoterpene photoxidation (OH and O_3 reaction), C*=0.1 μg m^{-3}	dark α-pinene ozonolysis (Saha and Grieshop, 2016, *ES&T*)	Xu et al., 2018, *ACP*
9	SVMT3	gas	semivolatile gas from monoterpene photoxidation (OH and O_3 reaction), C*=1 μg m^{-3}	dark α-pinene ozonolysis (Saha and Grieshop, 2016, *ES&T*)	Xu et al., 2018, *ACP*

	Species	Phase	Description	Scientific Basis	Model Implementation
10	SVMT4	gas	semivolatile gas from monoterpene photoxidation (OH and O_3 reaction), C*=10 μg m^{-3}	dark α-pinene ozonolysis (Saha and Grieshop, 2016, *ES&T*)	Xu et al., 2018, *ACP*
11	SVMT5	gas	semivolatile gas from monoterpene photoxidation (OH and O_3 reaction), C*=100 μg m^{-3}	dark α-pinene ozonolysis (Saha and Grieshop, 2016, *ES&T*)	Xu et al., 2018, *ACP*
12	SVMT6	gas	semivolatile gas from monoterpene photoxidation (OH and O_3 reaction), C*=1000 μg m^{-3}	dark α-pinene ozonolysis (Saha and Grieshop, 2016, *ES&T*)	Xu et al., 2018, *ACP*
13	AORGH2OJ	particle	water associated with organic species of particulate matter	hygroscopicity parameters (Petters and Kreidenweis, 2007, *ACP*) as a function of degree of oxygenation (Lambe et al., 2011, *ACP*)	Pye et al., 2017, *ACP*
14	AAVB1J	particle	low volatility organic particulate matter from oxidation of anthropogenic VOCs (benzene, toluene, xylene, PAHs, alkanes)	GEOS-Chem VBS parameterization (Pye et al., 2010, *ACP*) for aromatics and PAHs with long-chain alkanes following Pye and Pouliot (2012, *ES&T*) but with Presto et al. (2010, *ES&T*) VBS fits; all underlying experimental datasets are the same as in *aero6*	Qin et al., *in prep.*
15	AAVB2J	particle	semivolatile organic particulate matter from oxidation of anthropogenic VOCs (benzene, toluene, xylene, PAHs, alkanes)	see AAVB1J	Qin et al., *in prep.*
16	AAVB3J	particle	semivolatile organic particulate matter from oxidation of anthropogenic VOCs (benzene, toluene, xylene, PAHs, alkanes)	see AAVB1J	Qin et al., *in prep.*
17	AAVB4J	particle	semivolatile organic particulate matter from oxidation of anthropogenic VOCs (benzene, toluene, xylene, PAHs, alkanes)	see AAVB1J	Qin et al., *in prep.*

	Species	Phase	Description	Scientific Basis	Model Implementation
18	SVAVB1	gas	low volatility organic gas from oxidation of anthropogenic VOCs (benzene, toluene, xylene, PAHs, alkanes)	see AAVB1J	Qin et al., *in prep.*
19	SVAVB2	gas	semivolatile organic gas from oxidation of anthropogenic VOCs (benzene, toluene, xylene, PAHs, alkanes)	see AAVB1J	Qin et al., *in prep.*
20	SVAVB3	gas	semivolatile organic gas from oxidation of anthropogenic VOCs (benzene, toluene, xylene, PAHs, alkanes)	see AAVB1J	Qin et al., *in prep.*
21	SVAVB4	gas	semivolatile organic gas from oxidation of anthropogenic VOCs (benzene, toluene, xylene, PAHs, alkanes)	see AAVB1J	Qin et al., *in prep.*
22	MTNO3	gas	organic nitrates from monoterpene oxidation	gas-phase SAPRC yields (should not be counted as gas-phase organic nitrate for evaluation purposes in CB6r3 mechanisms)	Pye et al., 2015, *ES&T*
23	AMTNO3J	particle	semivolatile organic nitrates from monoterpene oxidation	Fry et al. (2009, *ACP*) for vapor pressure of monoterpene organic nitrates	Pye et al., 2015, *ES&T*
24	AMTHYDJ	particle	organic pseudo-hydrolysis accretion product from monoterpene organic nitrates (AMTNO3J)	Boyd et al. (2015, *ACP*) for hydrolysis timescale for tertiary nitrates, but applied to all MTNO3 following Pye et al. (2015, *ES&T*)	Pye et al., 2015, *ES&T*

*Species in AERO6/6i that are deprecated in AERO7/7i (these species should NOT appear in an AERO7/7i namelist): ATRP1J, ATRP2J, SV_TRP1, SV_TRP2, ABNZ1J, ABNZ2J, ABNZ3J, SV_BNZ1, SV_BNZ2, AXYL1J, AXYL2J, AXYL3J, SV_XYL1, SV_XYL2, ATOL1J, ATOL2J, ATOL3J, SV_TOL1, SV_TOL2, APAH1J, APAH2J, APAH3J, SV_PAH1, SV_PAH2, AALK1J, AALK2J, SV_ALK1, SV_ALK2

Table S2. Namelist options used for WRF version 3.8 simulation.

```
&time_control
 start_year                          = 2015,
 start_month                         = 12,
 start_day                           = 21,
 start_hour                          = 00,
 start_minute                        = 00,
 start_second                        = 00,
 end_year                            = 2015,
 end_month                           = 12,
 end_day                             = 27,
 end_hour                            = 00,
 end_minute                          = 01,
 end_second                          = 00,
 interval_seconds                    = 10800,
 input_from_file                     = .true.,
 history_interval                    = 60,
 frames_per_outfile                  = 24,
 restart                             = .FALSE.,
 restart_interval                    = 1440,
 io_form_history                     = 2
 io_form_restart                     = 2
 io_form_input                       = 2
 io_form_boundary                    = 2
 debug_level                         = 0
 io_form_auxinput2                   = 2
 io_form_auxinput4                   = 2
 auxinput1_inname                    = "metoa_em.d01.<date>"
 auxinput4_inname                    = "wrflowinp_d01"
 auxinput4_interval                  = 180
 auxinput4_end_h                     = 9025
 write_hist_at_0h_rst                = .true.,
 io_form_auxinput8                   = 2,
 auxinput8_inname                    = 'LTNG_<year>_<month>.nc',
 frames_per_auxinput8                = 1600,
 auxinput8_interval_m                = 30,
 auxinput8_end_h                     = 9999,
/

 &domains
 time_step                           = 60,
 time_step_fract_num                 = 0,
 time_step_fract_den                 = 1,
 use_adaptive_time_step              = .false.
 max_dom                             = 1,
 s_we                                = 1,
 e_we                                = 472,
 s_sn                                = 1,
 e_sn                                = 312,
 s_vert                              = 1,
 e_vert                              = 36,
 p_top_requested                     = 5000,
 eta_levels                          = 1.000, 0.9975, 0.995, 0.990, 0.985,
                                     0.980, 0.970, 0.960, 0.950,
                                     0.940, 0.930, 0.920, 0.910,
```

```
                        0.900, 0.880, 0.860, 0.840,
                        0.820, 0.800, 0.770, 0.740,
                        0.700, 0.650, 0.600, 0.550,
                        0.500, 0.450, 0.400, 0.350,
                        0.300, 0.250, 0.200, 0.150,
                        0.100, 0.050, 0.000
num_metgrid_levels              = 40,
dx                          = 12000,
dy                          = 12000,
grid_id                       = 1,
parent_id                     = 0,
i_parent_start                = 0,
j_parent_start                = 0,
parent_grid_ratio               = 1,
parent_time_step_ratio            = 1,
feedback                      = 1,
smooth_option                   = 0,
/

&physics
mp_physics                    = 10,
ra_lw_physics                 = 4,
ra_sw_physics                 = 4,
radt                        = 20,
sf_sfclay_physics               = 7,
sf_surface_physics              = 7,
bl_pbl_physics                = 7,
bldt                        = 0,
cu_physics                    = 1,
kfeta_trigger                 = 1,
cudt                         = 10,
ltg_assim                     = .true.,
suppress_opt                    = 2,
isfflx                      = 1,
ifsnow                        = 1,
icloud                       = 1,
cu_rad_feedback                 = .true.,
surface_input_source              = 1,
num_soil_layers                 = 2,
sst_update                    = 1,
pxlsm_smois_init                = 1,
slope_rad                     = 1,
topo_shading                    = 1,
shadlen                      = 25000.,
num_land_cat                    = 40,
prec_acc_dt                   = 60,
mp_zero_out                     = 2,
fractional_seaice               = 1,
seaice_threshold                = 0.0,
/

&fdda
grid_fdda                     = 1,
grid_sfdda                    = 1,
pxlsm_soil_nudge                = 1,
sgfdda_inname                   = "wrfsfdda_d01",
```

```
sgfdda_end_h                        = 9025,
sgfdda_interval_m                   = 180,
sgfdda_interval                     = 10800,
gfdda_inname                        = "wrffdda_d<domain>",
gfdda_end_h                         = 9025,
gfdda_interval_m                    = 180,
fgdt                                = 0,
if_no_pbl_nudging_uv                = 1,
if_no_pbl_nudging_t                 = 1,
if_no_pbl_nudging_q                 = 1,
if_zfac_uv                          = 0,
 k_zfac_uv                          = 13,
if_zfac_t                           = 0,
 k_zfac_t                           = 13,
if_zfac_q                           = 0,
 k_zfac_q                           = 13,
guv                                 = 0.0001,
gt                                  = 0.0001,
gq                                  = 0.00001,
guv_sfc                             = 0.0000,
gt_sfc                              = 0.0000,
gq_sfc                              = 0.0000,
if_ramping                          = 0,
dtramp_min                          = 60.0,
io_form_gfdda                       = 2,
rinblw                              = 250.0
/

&dynamics
w_damping                           = 1,
diff_opt                            = 1,
km_opt                              = 4,
diff_6th_opt                        = 2,
diff_6th_factor                     = 0.12,
damp_opt                            = 3,
base_temp                           = 290.
zdamp                               = 5000.,
dampcoef                            = 0.05,
khdif                               = 0,
kvdif                               = 0,
non_hydrostatic                     = .true.,
moist_adv_opt                       = 2,
tke_adv_opt                         = 2,
scalar_adv_opt                      = 2,
/

&dfi_control
dfi_opt                             = 0
dfi_nfilter                         = 7
dfi_write_filtered_input            = .true.
dfi_write_dfi_history               = .false.
dfi_cutoff_seconds                  = 60
dfi_time_dim                        = 1000
dfi_bckstop_year                    = 2006
dfi_bckstop_month                   = 08
dfi_bckstop_day                     = 04
```

```
dfi_bckstop_hour                    = 12
dfi_bckstop_minute                  = 00
dfi_bckstop_second                  = 00
dfi_fwdstop_year                    = 2006
dfi_fwdstop_month                   = 08
dfi_fwdstop_day                     = 04
dfi_fwdstop_hour                    = 13
dfi_fwdstop_minute                  = 00
dfi_fwdstop_second                  = 00
/

&bdy_control
spec_bdy_width                      = 5,
spec_zone                           = 1,
relax_zone                          = 4,
specified                           = .true.,
nested                              = .false.,
/

&grib2
/

&namelist_quilt
nio_tasks_per_group = 0,
nio_groups = 1,
/
```

Table S3. Namelist options used in WRF version 4.1.1 simulation.

```
&time_control
 start_year                          = $YS
 start_month                         = $MS
 start_day                           = $DS
 start_hour                          = 00
 start_minute                        = 00,
 start_second                        = 00,
 end_year                            = $YE
 end_month                           = $ME
 end_day                             = $DE
 end_hour                            = 00
 end_minute                          = 00,
 end_second                          = 00,
 interval_seconds                    = 10800
 input_from_file                     = .true.,
 history_interval                    = 60,
 frames_per_outfile                  = 24,
 restart                             = .true.
 restart_interval                    = 1440,
 write_hist_at_0h_rst                = .true.,
 io_form_history                     = 2
 io_form_restart                     = 2
 io_form_input                       = 2
 io_form_boundary                    = 2
 io_form_auxinput2                   = 2
 io_form_auxinput4                   = 2
 io_form_auxinput8                   = 2,
 debug_level                         = 0
 auxinput1_inname                    = "met_em.d01.<date>"
 auxinput4_inname                    = "wrflowinp_d01"
 auxinput4_interval                  = 180
 auxinput4_end_h                     = 999999999
 auxinput8_inname                    = "LIGHTNING"
 auxinput8_interval                  = 30
 auxinput8_end_h                     = 999999999
 frames_per_auxinput8                = 7344,
 reset_simulation_start              = .false.,
 iofields_filename                   = "output.var.txt"
 force_use_old_data                  = .true.
/

 &domains
 time_step                           = 60,
 time_step_fract_num                 = 0,
 time_step_fract_den                 = 1,
 max_dom                             = 1,
 s_we                                = 1,
 e_we                                = 472,
 s_sn                                = 1,
 e_sn                                = 312,
 s_vert                              = 1,
 e_vert                              = 36,
 p_top_requested                     = 5000,
 eta_levels                          = 1.000, 0.9975, 0.995, 0.990, 0.985,
```

```
                            0.980, 0.970, 0.960, 0.950,
                            0.940, 0.930, 0.920, 0.910,
                            0.900, 0.880, 0.860, 0.840,
                            0.820, 0.800, 0.770, 0.740,
                            0.700, 0.650, 0.600, 0.550,
                            0.500, 0.450, 0.400, 0.350,
                            0.300, 0.250, 0.200, 0.150,
                            0.100, 0.050, 0.000
 num_metgrid_levels              = 40,
 dx                             = 12000,
 dy                             = 12000,
 grid_id                         = 1,
 parent_id                       = 0,
 i_parent_start                  = 0,
 j_parent_start                  = 0,
 parent_grid_ratio               = 1,
 parent_time_step_ratio          = 1,
 feedback                        = 1,
 smooth_option                   = 0,
 /

 &physics
 mp_physics                      = 10,
 mp_zero_out                     = 2,
 mp_zero_out_thresh              = 1.0e-8,
 ra_lw_physics                   = 4,
 ra_sw_physics                   = 4,
 radt                           = 20,
 co2tf                           = 1,
 sf_sfclay_physics               = 7,
 num_soil_layers                 = 2,
 pxlsm_smois_init                = 0,
 pxlsm_modis_veg                 = 1,
 sf_surface_physics              = 7,
 sf_urban_physics                = 0,
 bl_pbl_physics                  = 7,
 bldt                           = 0,
 cu_physics                      = 1,
 kfeta_trigger                   = 1,
 cudt                            = 0,
 prec_acc_dt                     = 60,
 isfflx                         = 1,
 ifsnow                          = 1,
 icloud                          = 1,
 cu_rad_feedback                 = .true.,
 surface_input_source            = 1,
 num_land_cat                    = 40,
 num_soil_cat                    = 16,
 sst_update                      = 1,
 seaice_threshold                = 100,
 slope_rad                       = 1,
 topo_shading                    = 1,
 shadlen                         = 25000.,
 do_radar_ref                    = 1,
 grav_settling                   = 0,
 ltg_assim                       = .true.,
```

```
suppress_opt                        = 2,
/

&fdda
grid_fdda                           = 1,
grid_sfdda                          = 1,
pxlsm_soil_nudge                    = 1,
sgfdda_inname                       = "wrfsfdda_d01",
sgfdda_end_h                        = 999999999,
sgfdda_interval_m                   = 180,
gfdda_inname                        = "wrffdda_d<domain>",
gfdda_end_h                         = 999999999,
gfdda_interval_m                    = 180,
fgdt                                = 0,
if_no_pbl_nudging_uv                = 1,
if_no_pbl_nudging_t                 = 1,
if_no_pbl_nudging_q                 = 1,
if_zfac_uv                          = 0,
 k_zfac_uv                          = 13,
if_zfac_t                           = 0,
 k_zfac_t                           = 13,
if_zfac_q                           = 0,
 k_zfac_q                           = 13,
guv                                 = 0.0001,
gt                                  = 0.0001,
gq                                  = 0.00001,
guv_sfc                             = 0.0000,
gt_sfc                              = 0.0000,
gq_sfc                              = 0.0000,
if_ramping                          = 1,
dtramp_min                          = 60.0,
io_form_gfdda                       = 2,
rinblw                              = 250.0
/

&dynamics
hybrid_opt                          = 2,
w_damping                           = 1,
diff_opt                            = 1,
km_opt                              = 4,
diff_6th_opt                        = 2,
diff_6th_factor                     = 0.12,
damp_opt                            = 3,
base_temp                           = 290.
zdamp                               = 5000.,
dampcoef                            = 0.05,
khdif                               = 0,
kvdif                               = 0,
non_hydrostatic                     = .true.,
moist_adv_opt                       = 2,
tke_adv_opt                         = 2,
scalar_adv_opt                      = 2,
/

&bdy_control
spec_bdy_width                      = 5,
```

```
spec_zone                  = 1,
relax_zone                 = 4,
specified                  = .true.,
spec_exp                   = 0.0,
nested                     = .false.,
/

&grib2
/

&namelist_quilt
nio_tasks_per_group = 0,
nio_groups = 1,
```

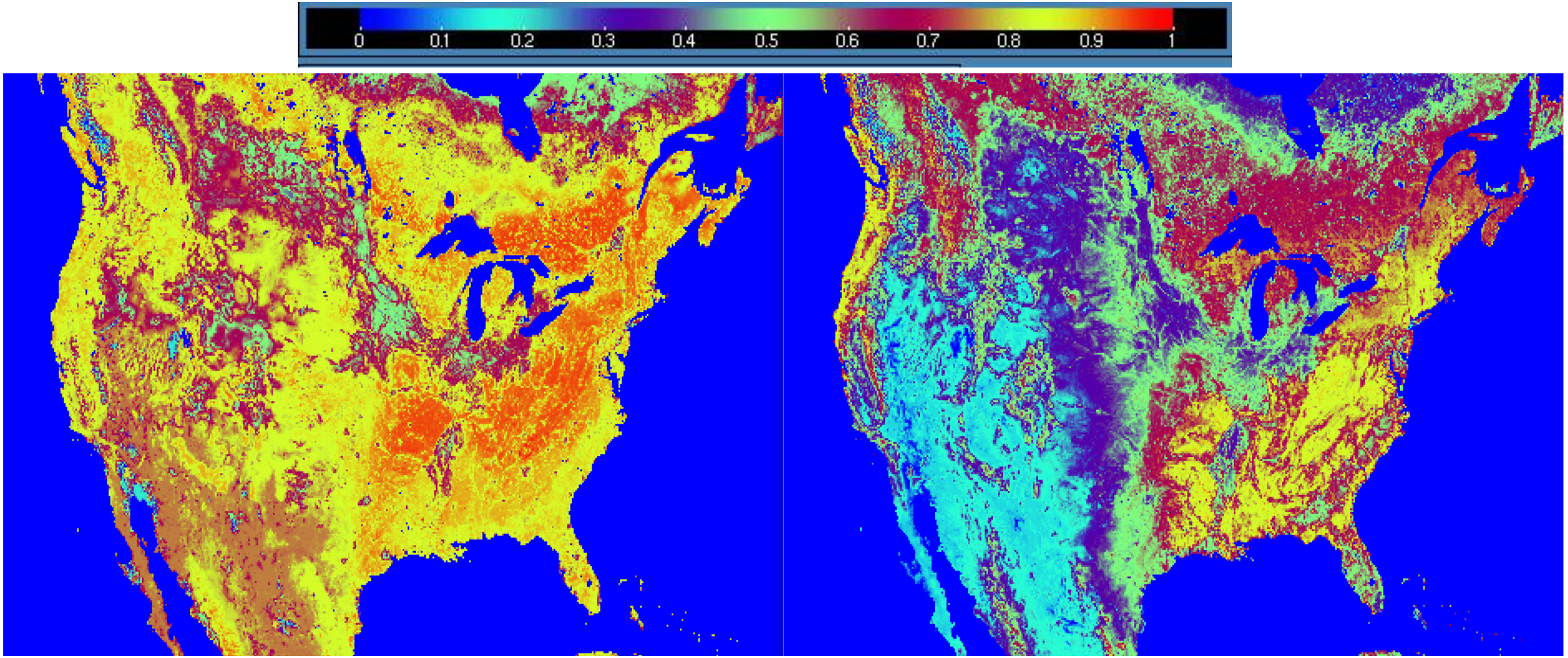

Figure S1. Vegetation Fraction (VF) on June 1, 2016 from WRF38 (left) and WRF411 (right).

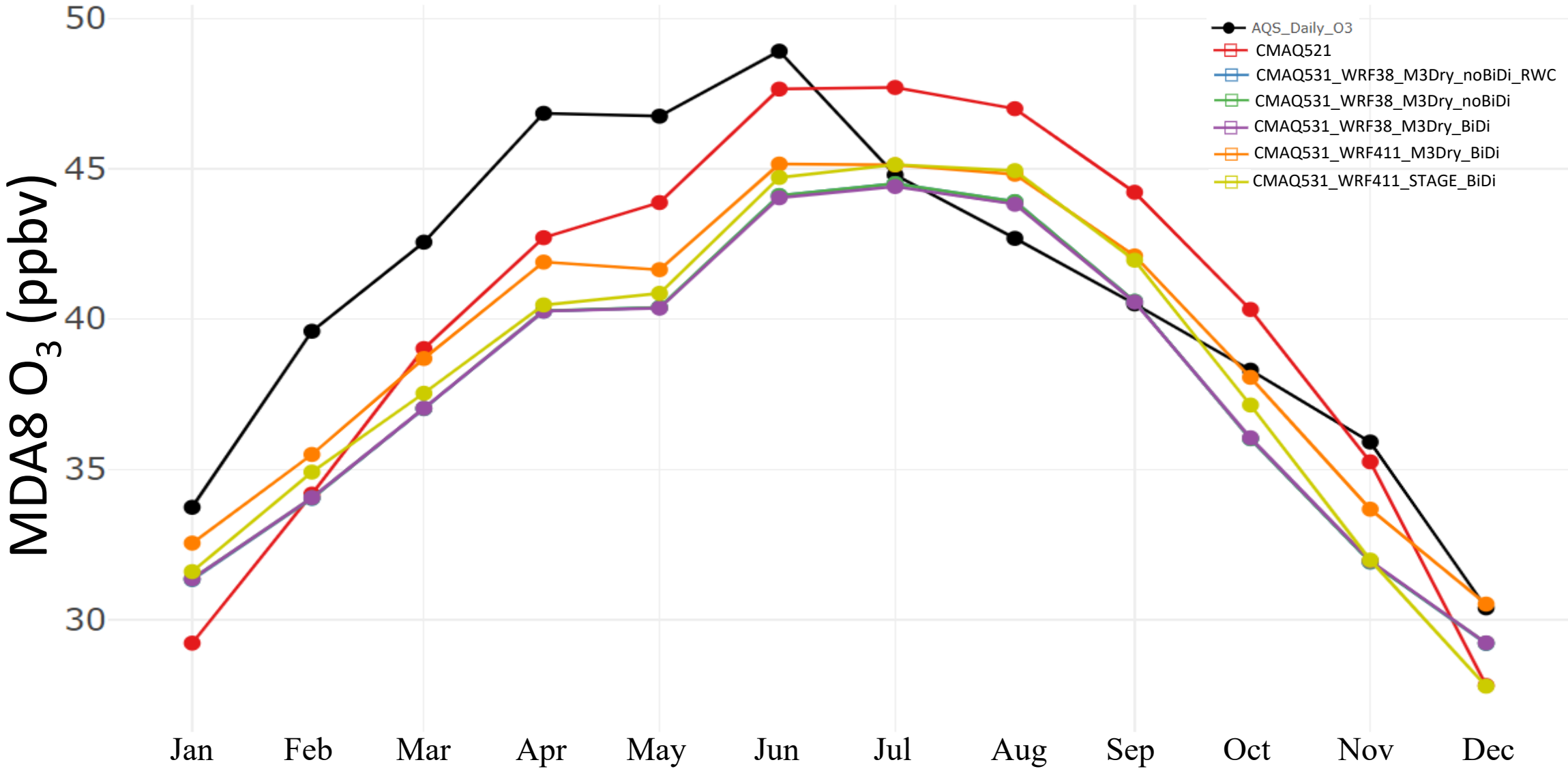

Figure S2. Time series of monthly average MDA8 O_3 mixing ratio (ppbv) for all AQS sites (black), CMAQ521 (red), CMAQ531_WRF38_M3Dry_noBiDi_RWC (blue), CMAQ531_WRF38_M3Dry_noBiDi (green), CMAQ531_WRF38_M3Dry_BiDi (purple), CMAQ531_WRF411_M3Dry_BiDi (orange), and CMAQ531_WRF411_STAGE_BiDi (yellow).

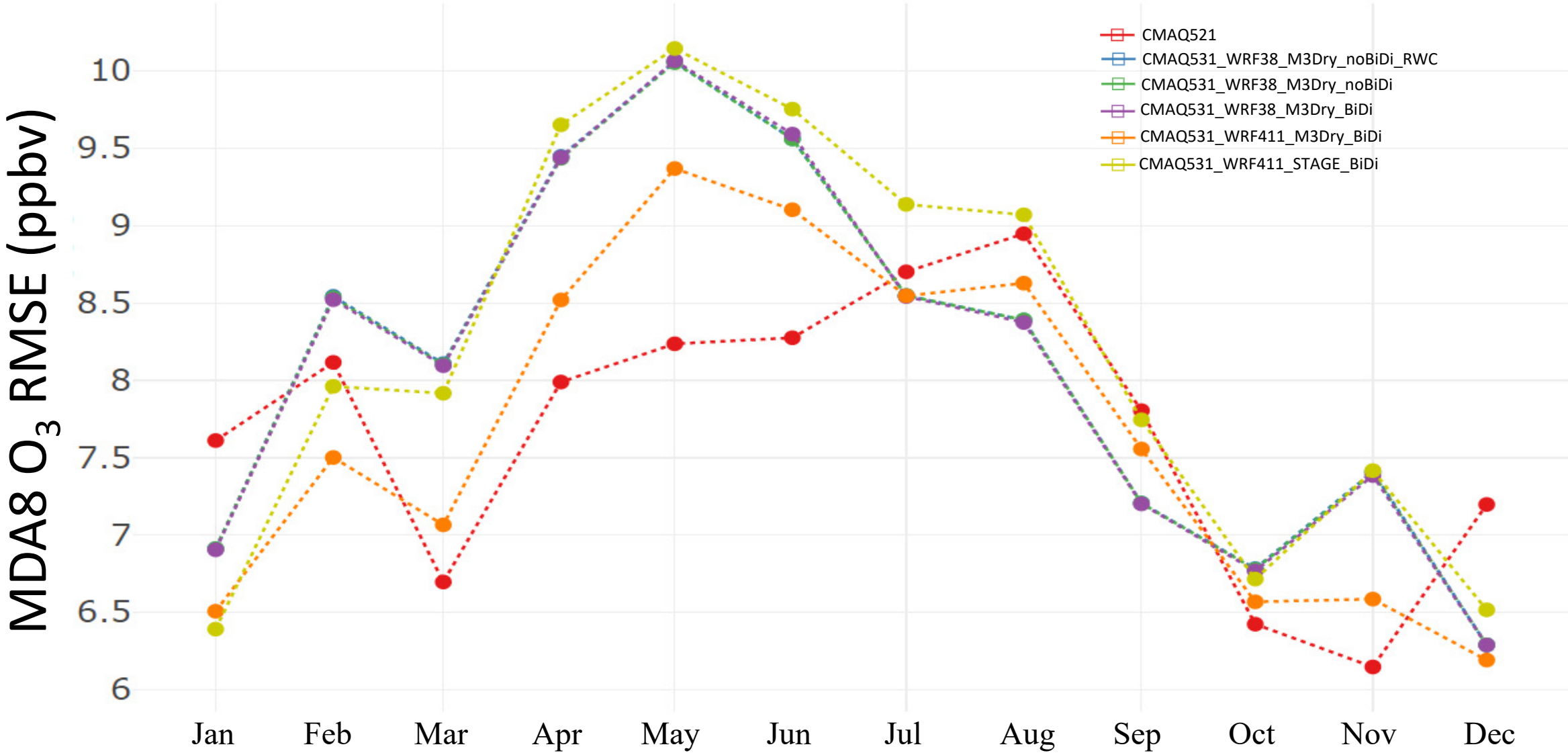

Figure S3. Time series of monthly average MDA8 O_3 RMSE (ppbv) for all AQS sites for CMAQ521 (red), CMAQ531_WRF38_M3Dry_noBiDi_RWC (blue), CMAQ531_WRF38_M3Dry_noBiDi (green), CMAQ531_WRF38_M3Dry_BiDi (purple), CMAQ531_WRF411_M3Dry_BiDi (orange), and CMAQ531_WRF411_STAGE_BiDi (yellow).

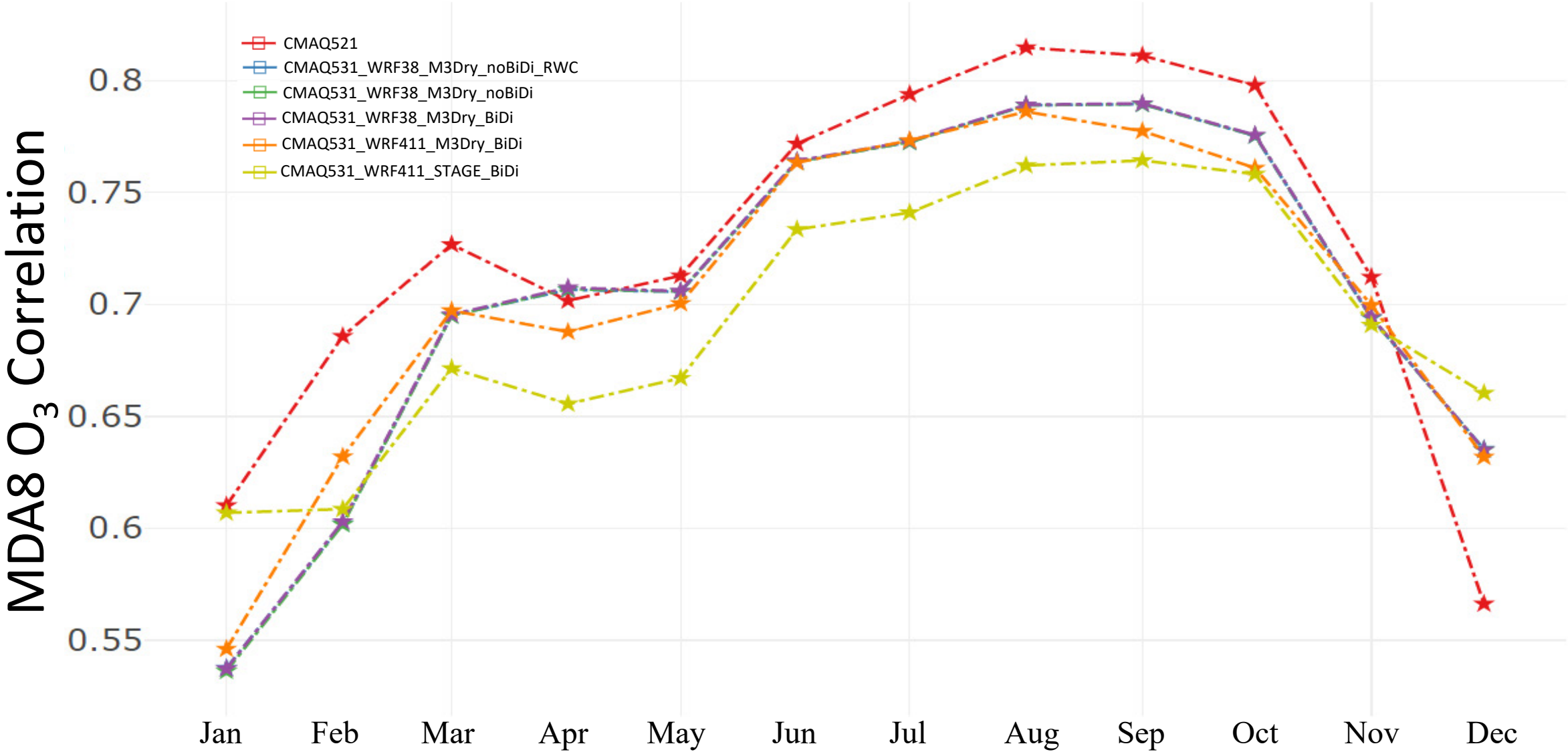

Figure S4. Time series of monthly average MDA8 O_3 Pearson correlation for all AQS sites for CMAQ521 (red), CMAQ531_WRF38_M3Dry_noBiDi_RWC (blue), CMAQ531_WRF38_M3Dry_noBiDi (green), CMAQ531_WRF38_M3Dry_BiDi (purple), CMAQ531_WRF411_M3Dry_BiDi (orange), and CMAQ531_WRF411_STAGE_BiDi (yellow).

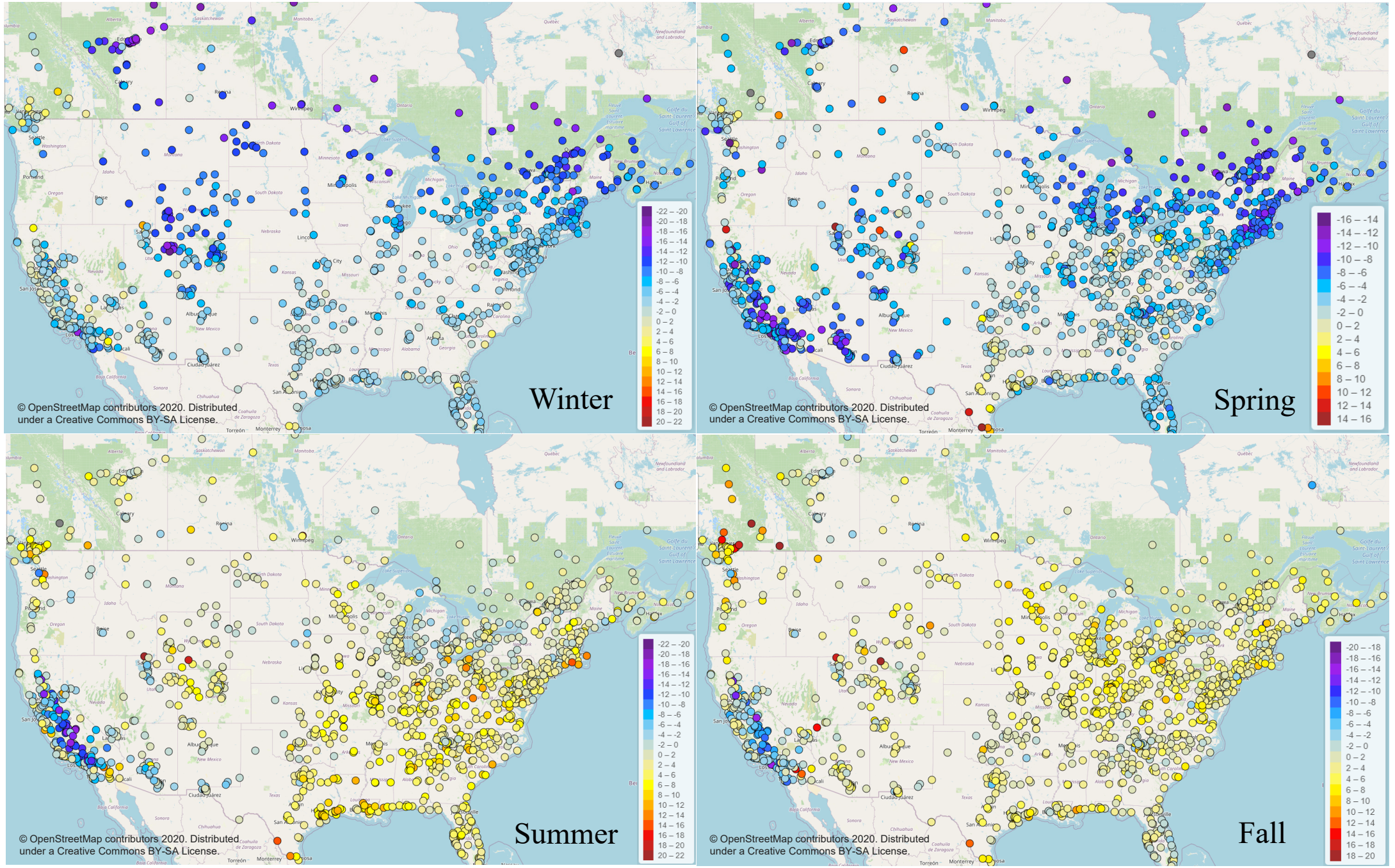

Figure S5. Seasonal average MDA8 O_3 bias (ppbv) for AQS and NAPS sites for the CMAQ521 simulation.

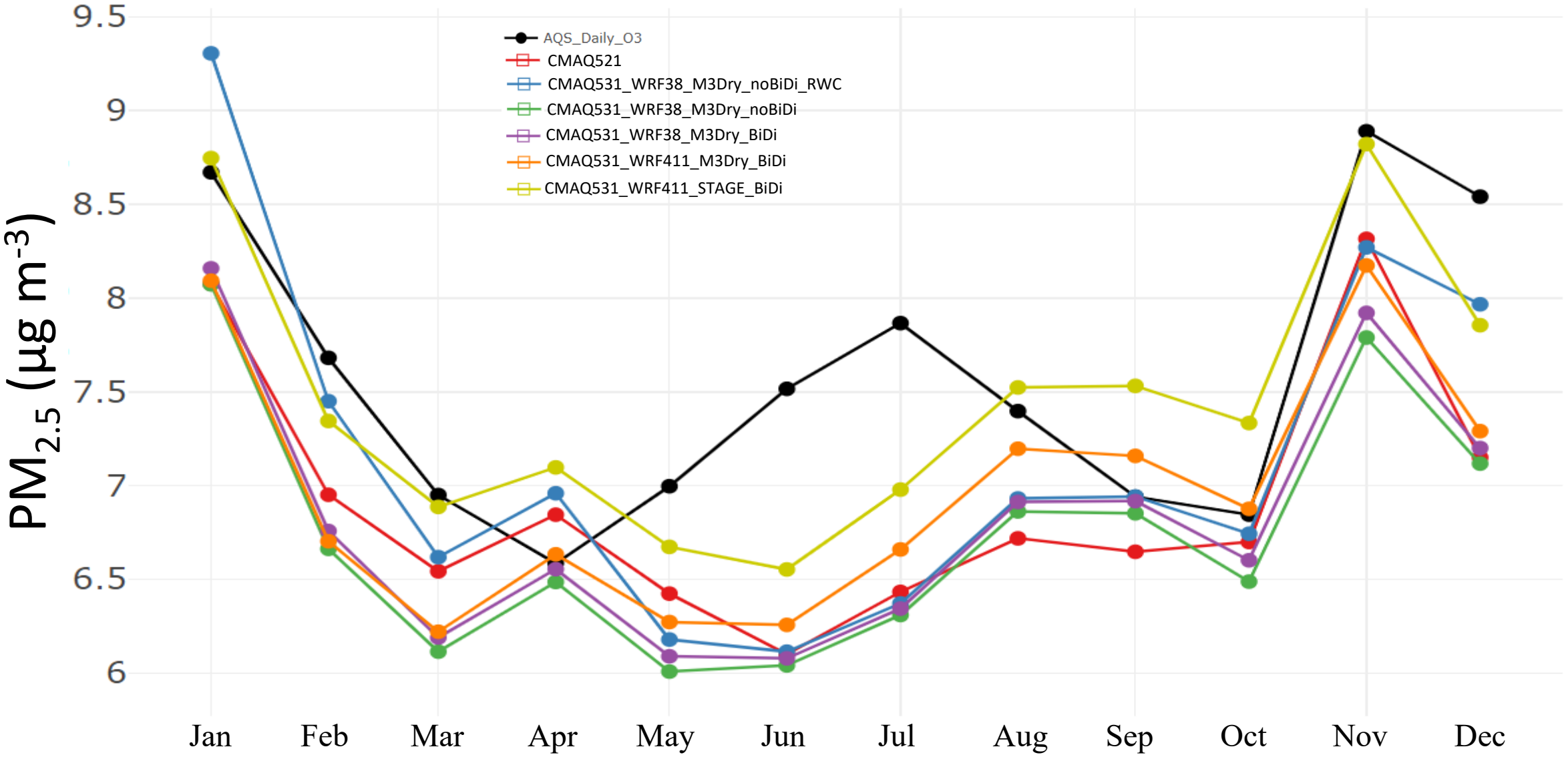

Figure S6. Time series of monthly average $PM_{2.5}$ (µg m^{-3}) for all AQS sites (black), CMAQ521 (red), CMAQ531_WRF38_M3Dry_noBiDi_RWC (blue), CMAQ531_WRF38_M3Dry_noBiDi (green), CMAQ531_WRF38_M3Dry_BiDi (purple), CMAQ531_WRF411_M3Dry_BiDi (orange), and CMAQ531_WRF411_STAGE_BiDi (yellow).

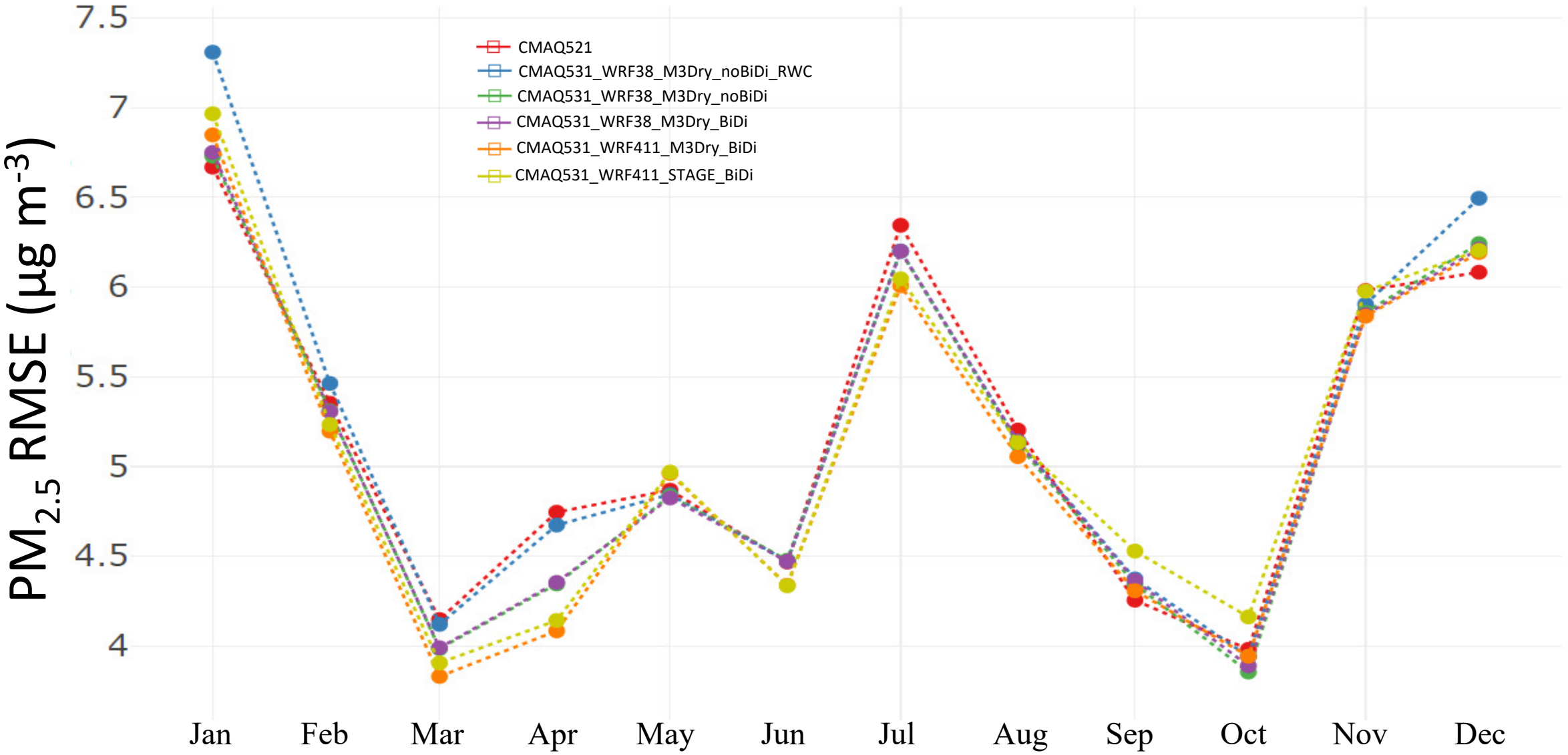

Figure S7. Time series of monthly average $PM_{2.5}$ RMSE (µg m^{-3}) for all AQS sites for CMAQ521 (red), CMAQ531_WRF38_M3Dry_noBiDi_RWC (blue), CMAQ531_WRF38_M3Dry_noBiDi (green), CMAQ531_WRF38_M3Dry_BiDi (purple), CMAQ531_WRF411_M3Dry_BiDi (orange), and CMAQ531_WRF411_STAGE_BiDi (yellow).

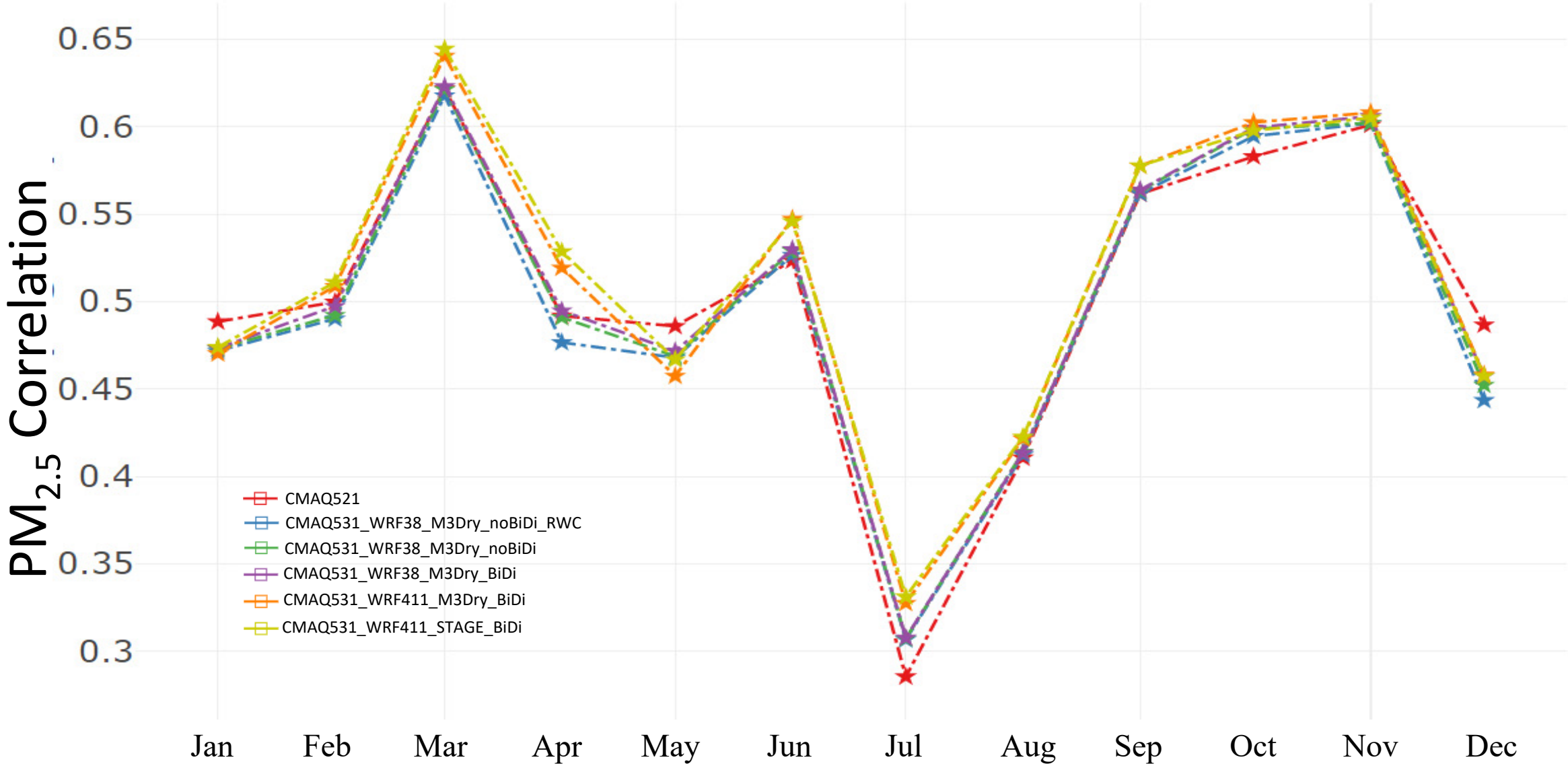

Figure S8. Time series of monthly average $PM_{2.5}$ Pearson correlation for all AQS sites for CMAQ521 (red), CMAQ531_WRF38_M3Dry_noBiDi_RWC (blue), CMAQ531_WRF38_M3Dry_noBiDi (green), CMAQ531_WRF38_M3Dry_BiDi (purple), CMAQ531_WRF411_M3Dry_BiDi (orange), and CMAQ531_WRF411_STAGE_BiDi (yellow).

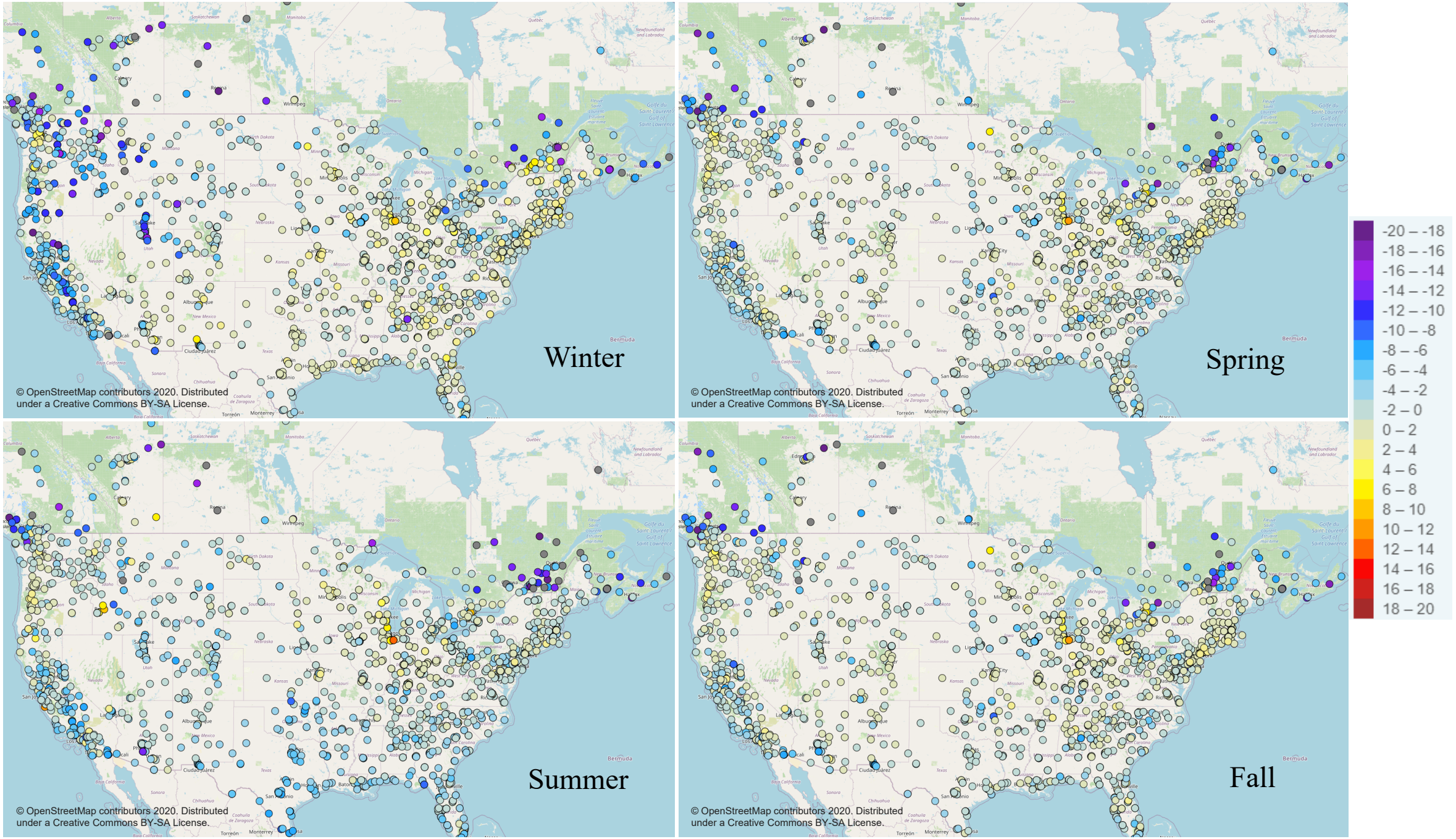

Figure S9. Seasonal average $PM_{2.5}$ bias ($\mu g\ m^{-3}$) for AQS and NAPS sites the CMAQ521 simulation.

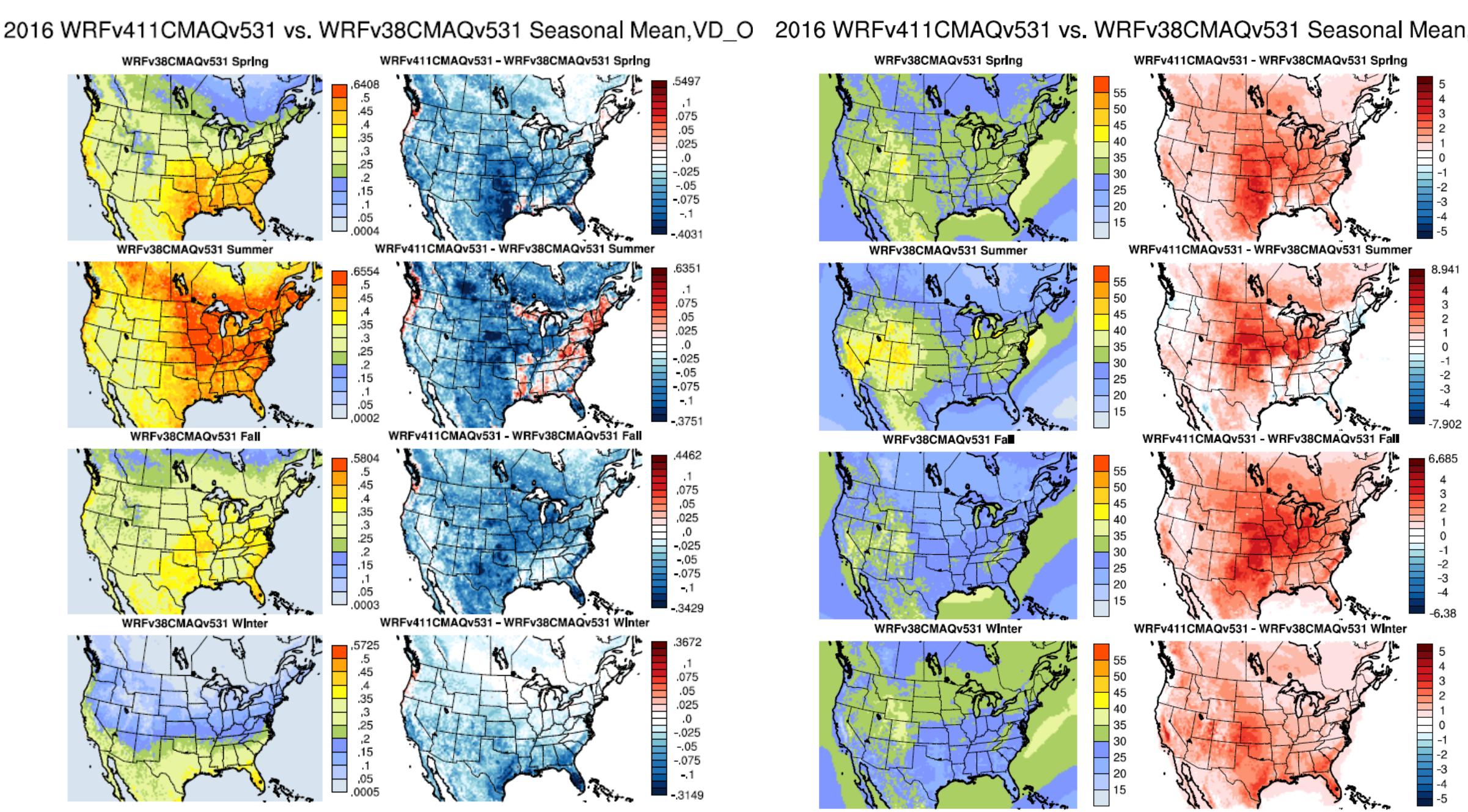

Figure S10. Seasonal O_3 deposition velocity (VD_O_3; left) and O_3 mixing ratio (ppbv) for the CMAQ531_WRF38_M3Dry_BiDi simulation along with the difference in VD_O_3 and mixing ratio between the CMAQ531_WRF38_M3Dry_Bidi and CMAQ531_WRF411_M3Dry_BiDi simulations (WRF411 – WRF38).

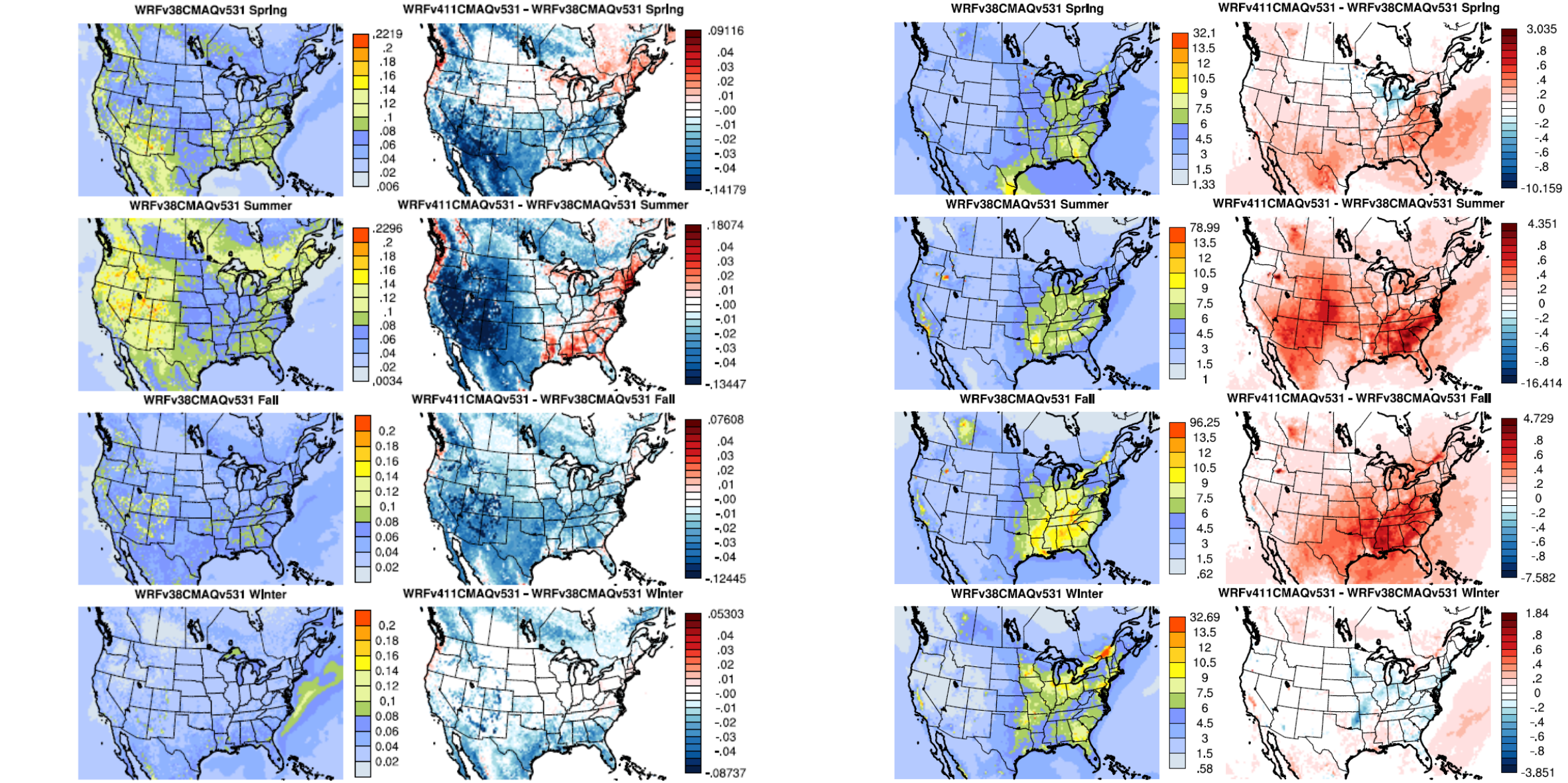

Figure S11. Seasonal accumulation mode deposition velocity (VMASSJ; left) and $PM_{2.5}$ concentration (µg m^{-3}) for the CMAQ531_WRF38_M3Dry_BiDi simulation along with the difference in VMASSJ and $PM_{2.5}$ concentration between the CMAQ531_WRF38_M3Dry_Bidi and CMAQ531_WRF411_M3Dry_BiDi simulations (WRF411 – WRF38).

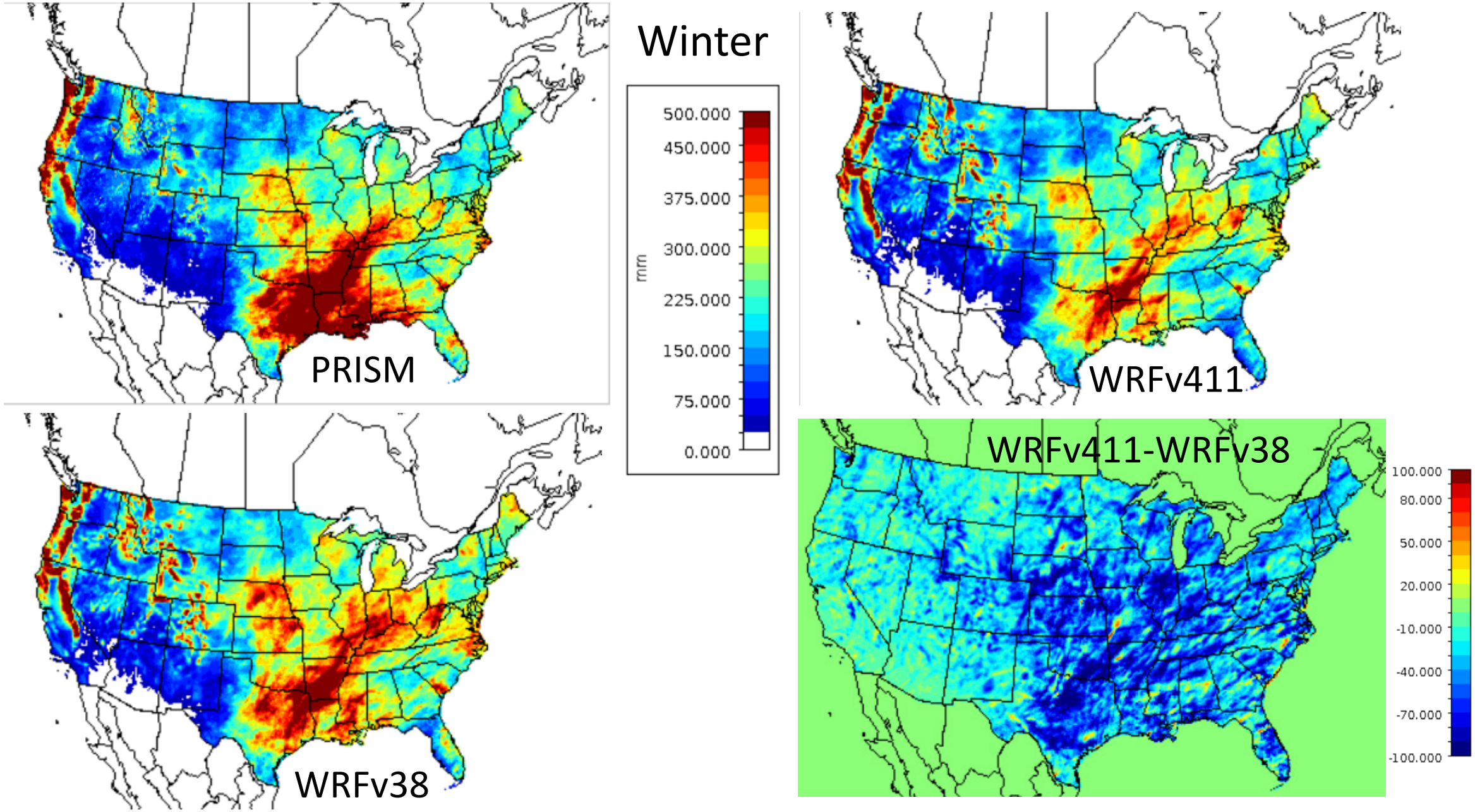

Figure S12. Observed and simulation precipitation for winter 2006 in mm. Observed precipitation from PRISM (upper left), WRFv411 simulated precipitation (upper right), WRFv38 simulated precipitation (lower left), and the difference between WRFv411 and WRFv38 (WRFv411 – WRFv38) precipitation (lower right).

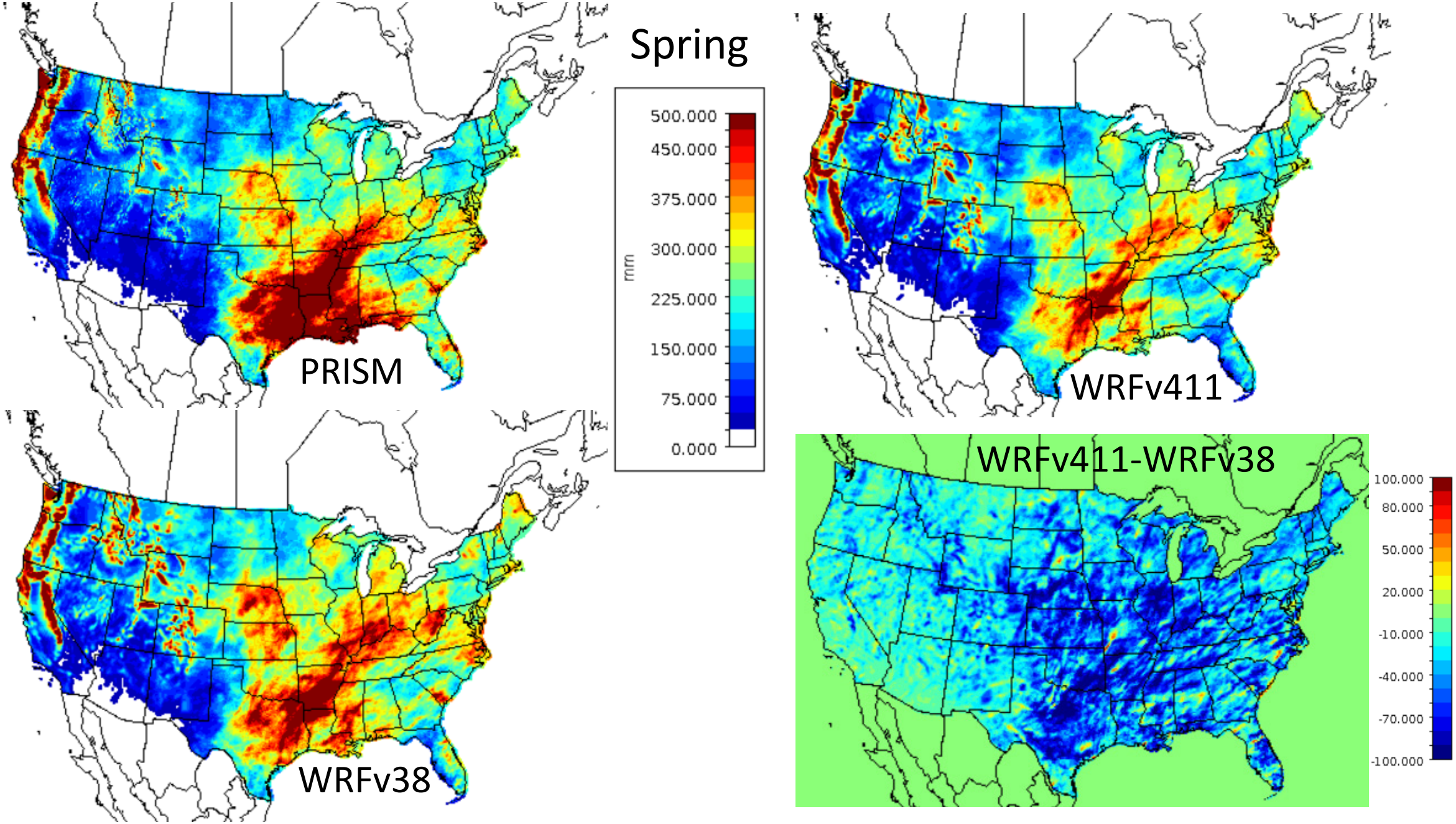

Figure S13. Observed and simulation precipitation for spring 2006 in mm. Observed precipitation from PRISM (upper left), WRFv411 simulated precipitation (upper right), WRFv38 simulated precipitation (lower left), and the difference between WRFv411 and WRFv38 (WRFv411 – WRFv38) precipitation (lower right).

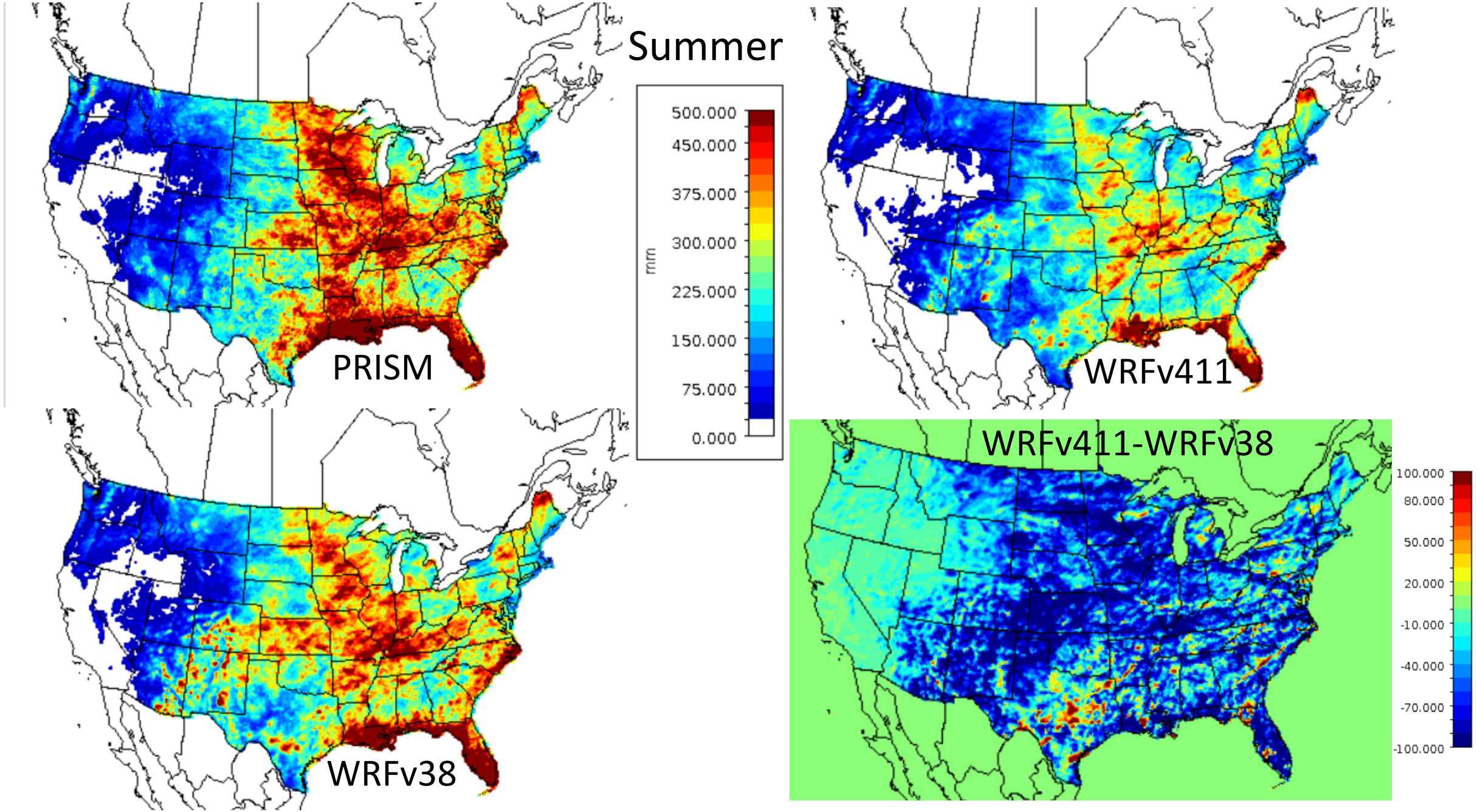

Figure S14. Observed and simulation precipitation for summer 2006 in mm. Observed precipitation from PRISM (upper left), WRFv411 simulated precipitation (upper right), WRFv38 simulated precipitation (lower left), and the difference between WRFv411 and WRFv38 (WRFv411 – WRFv38) precipitation (lower right).

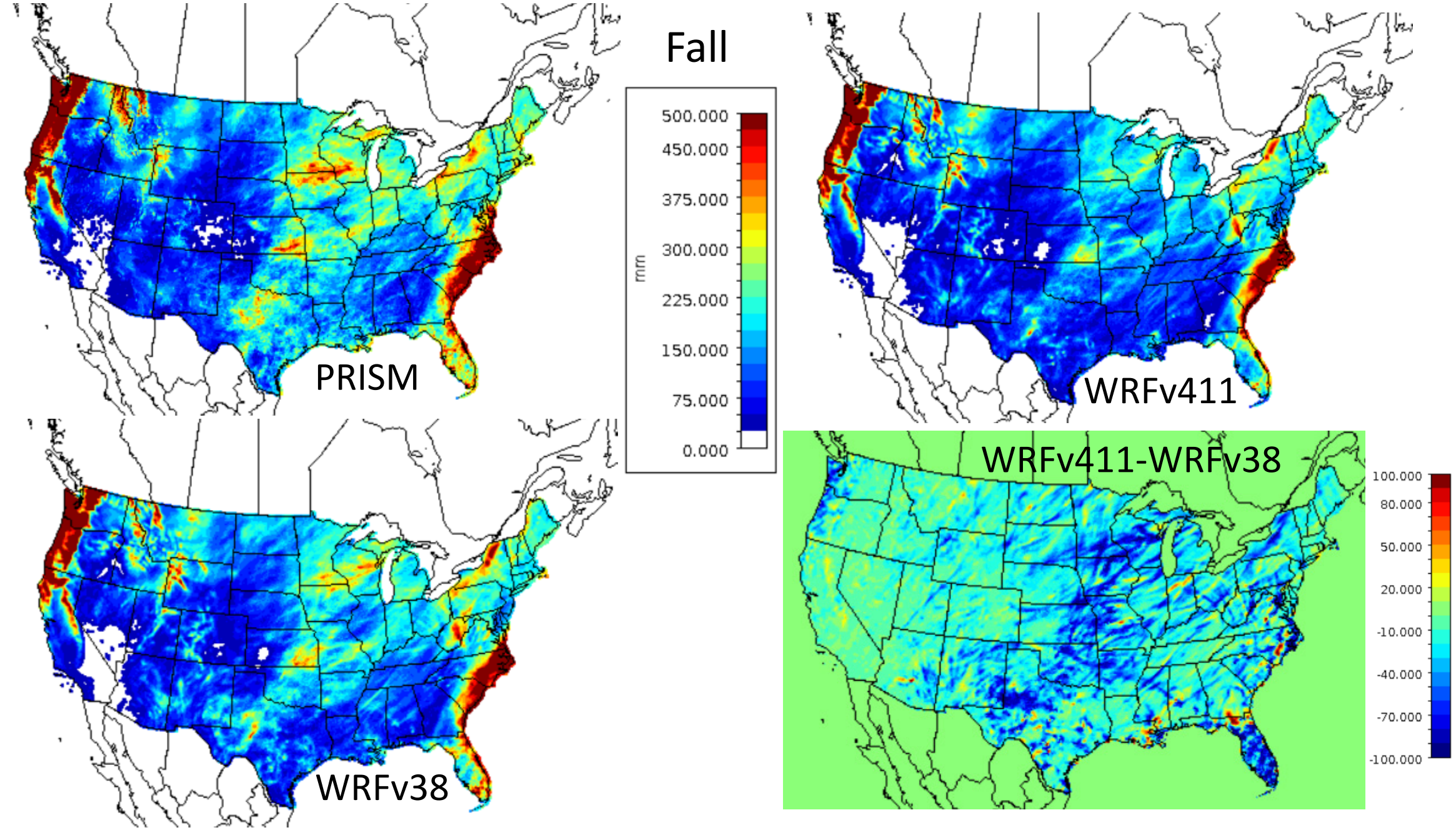

Figure S15. Observed and simulation precipitation for fall 2006 in mm. Observed precipitation from PRISM (upper left), WRFv411 simulated precipitation (upper right), WRFv38 simulated precipitation (lower left), and the difference between WRFv411 and WRFv38 (WRFv411 – WRFv38) precipitation (lower right).

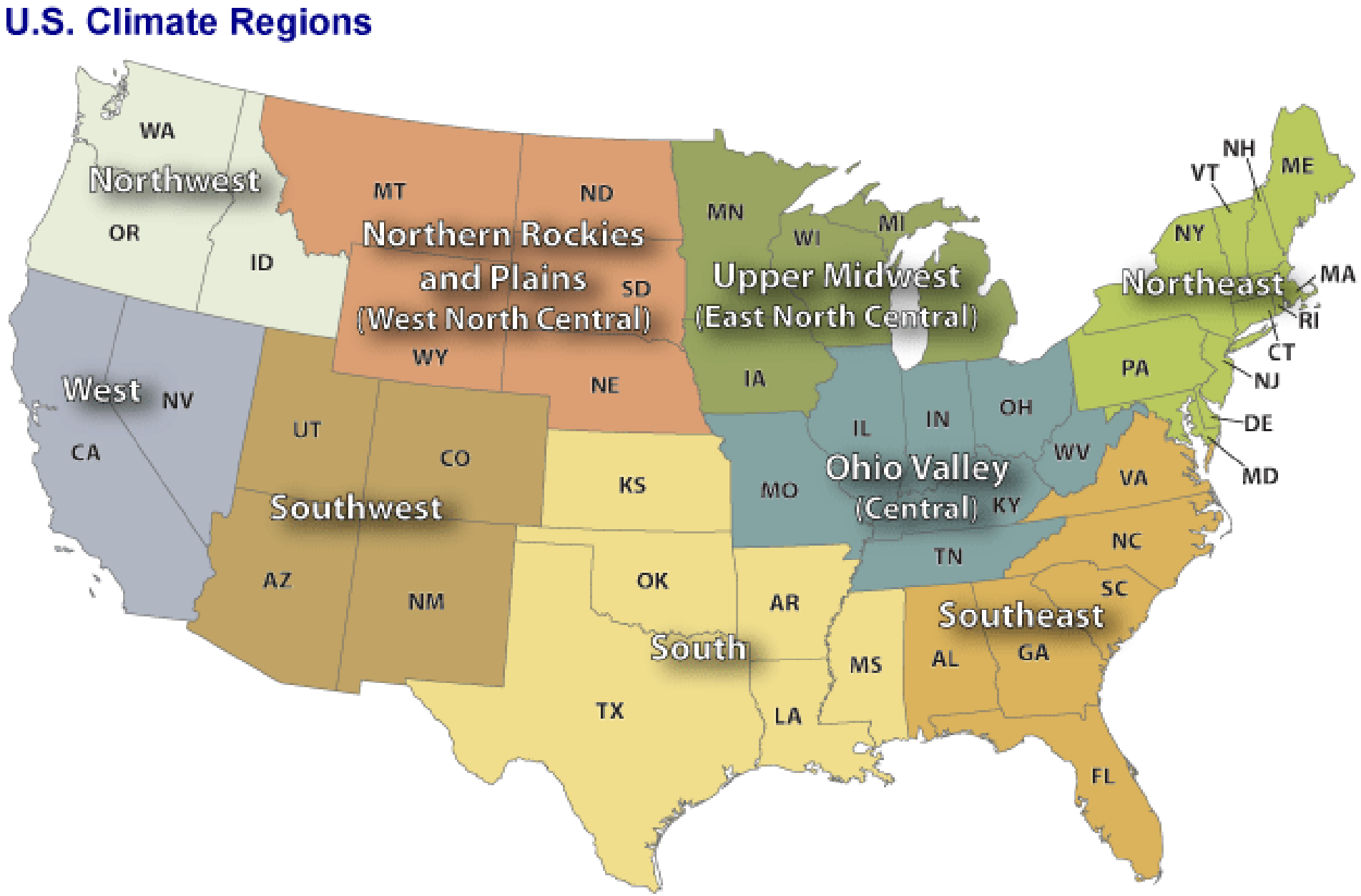

Figure S16. Map of the NOAA U.S. climate regions. Image source: https://www.ncdc.noaa.gov/monitoring-references/maps/us-climate-regions.php.

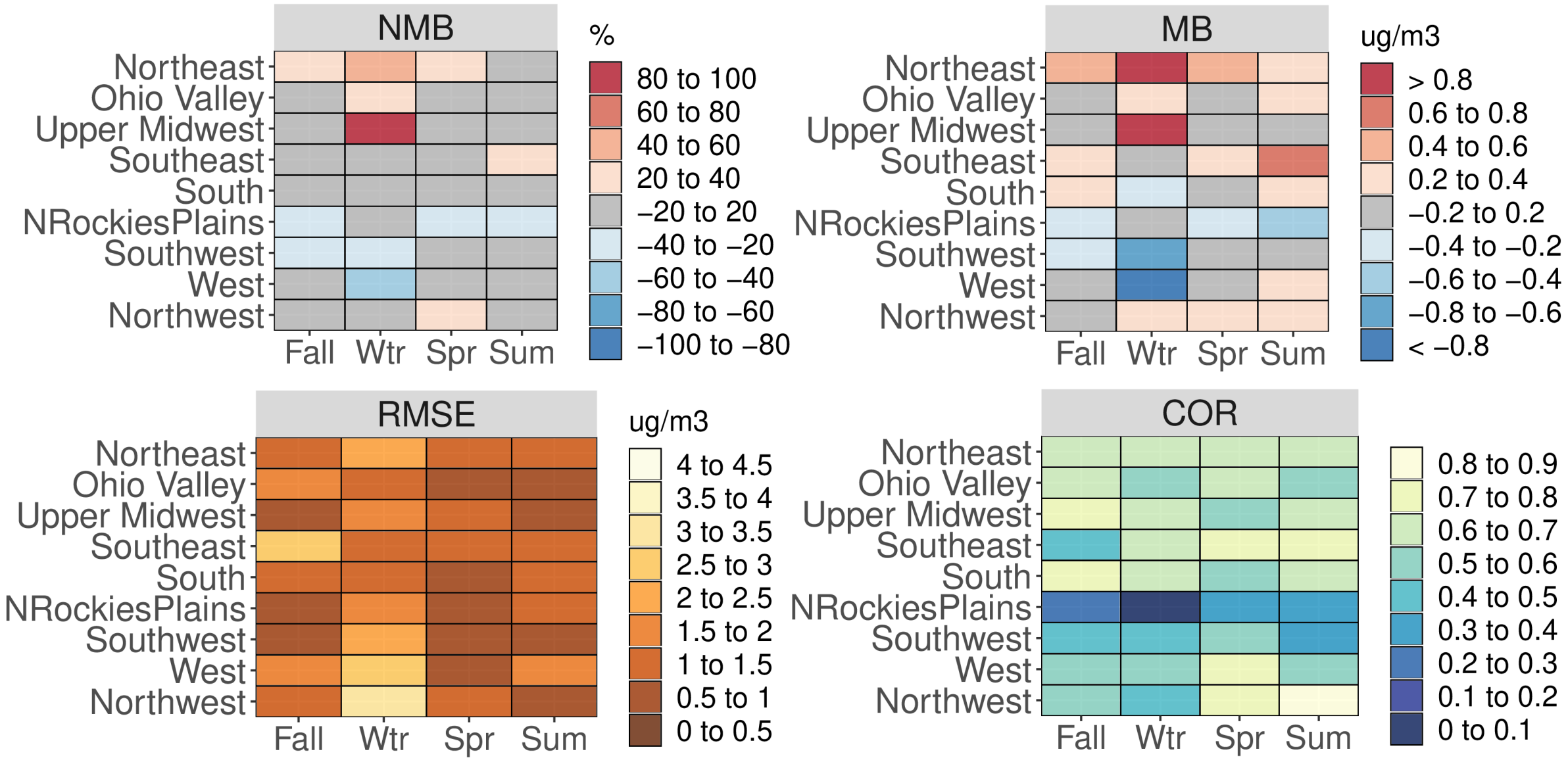

Figure S17. Categorical NMB (%), MB (μg m^{-3}), RMSE (μg m^{-3}), and Pearson correlation values for OC for all CSN sites based on season and NOAA climate region for the CMAQ531_WRF411_M3Dry_BiDi simulation.

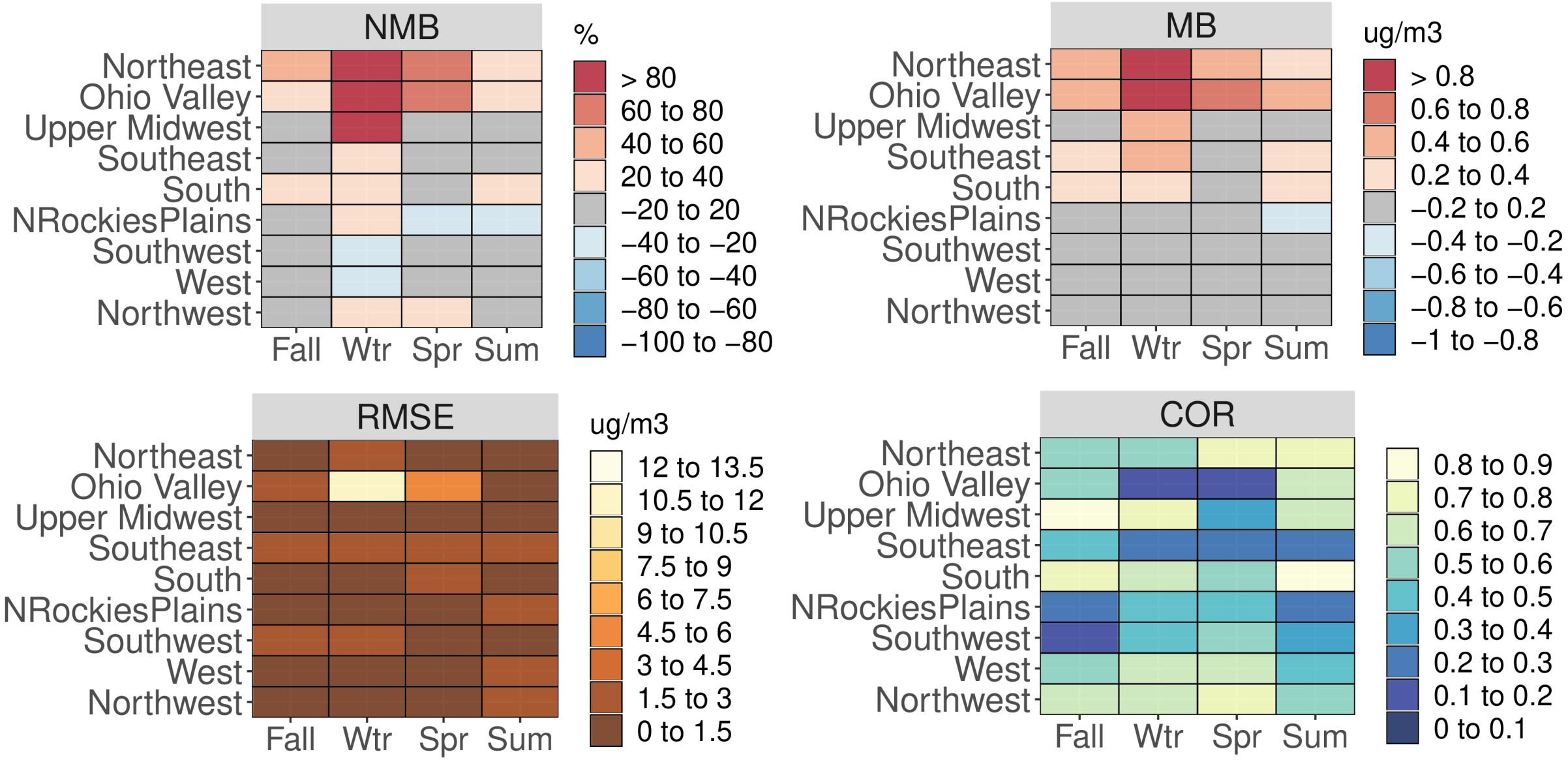

Figure S18. Categorical NMB (%), MB (μg m^{-3}), RMSE (μg m^{-3}), and Pearson correlation values for OC for all IMPROVE sites based on season and NOAA climate region for the CMAQ531_WRF411_M3Dry_BiDi simulation.

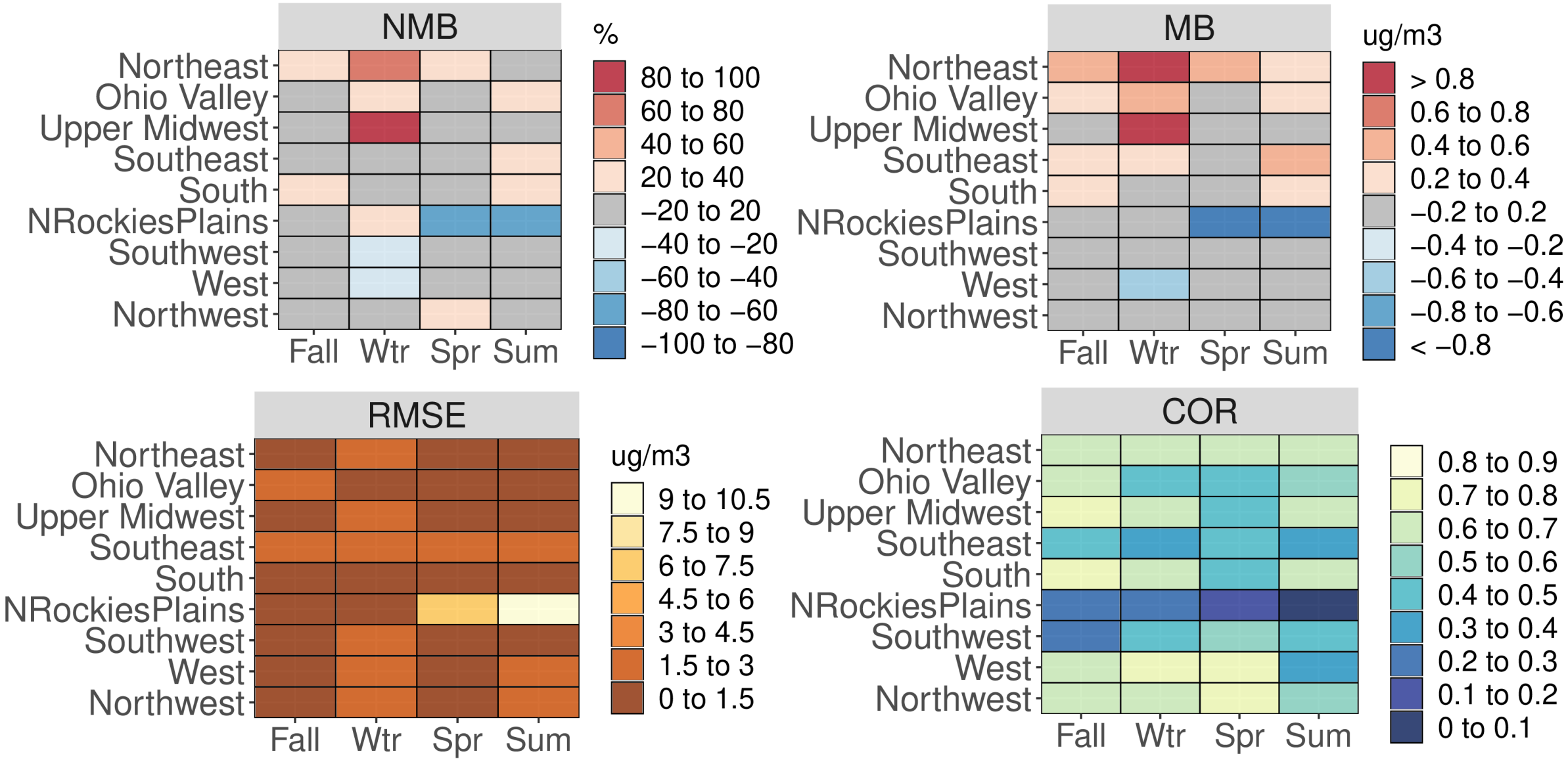

Figure S19. Categorical NMB (%), MB (μg m^{-3}), RMSE (μg m^{-3}), and Pearson correlation values for OC for all AQS sites based on season and NOAA climate region for the CMAQ531_WRF411_M3Dry_BiDi simulation.

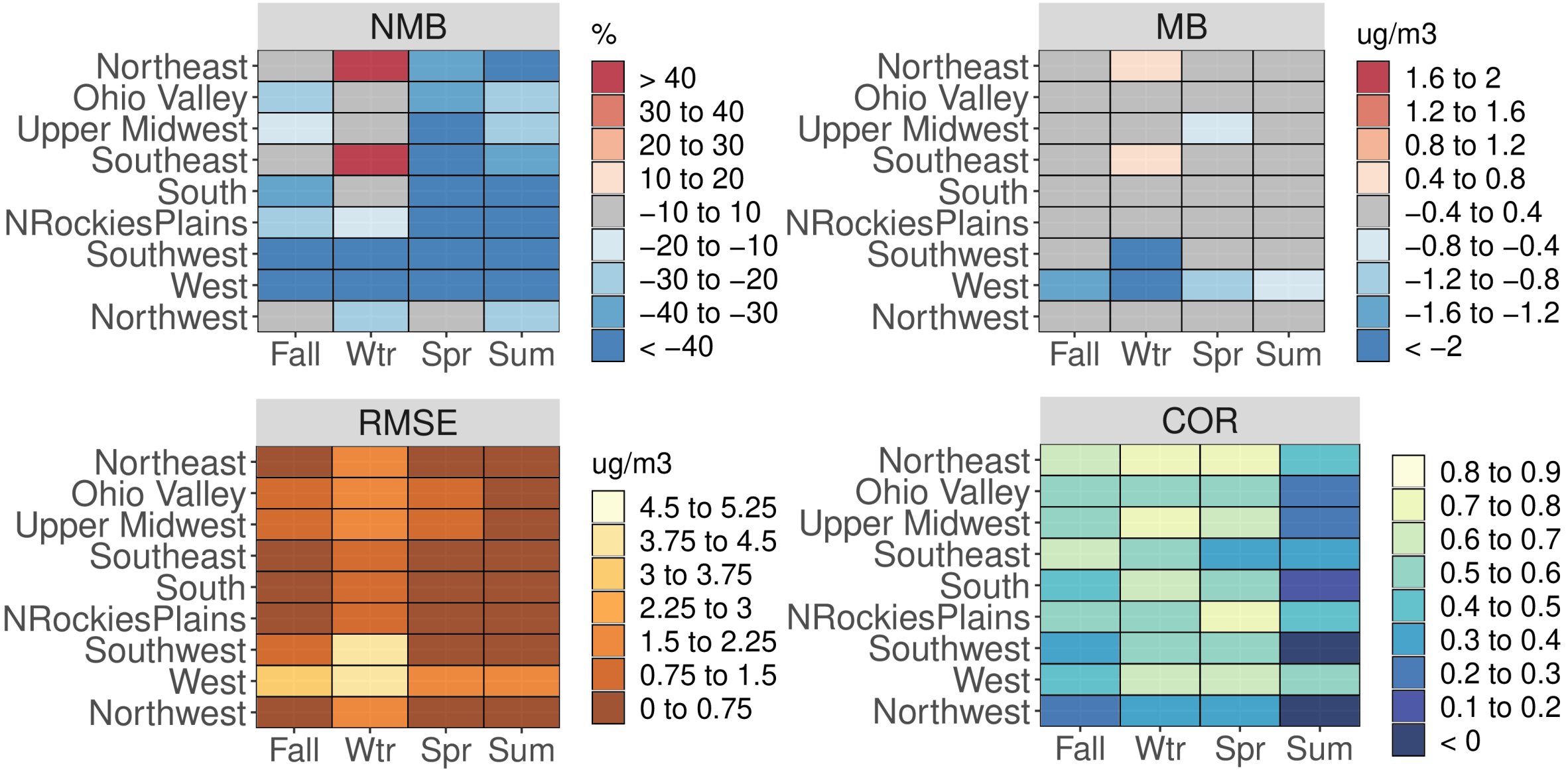

Figure S20. Categorical NMB (%), MB (μg m^{-3}), RMSE (μg m^{-3}), and Pearson correlation values for NO_3^- for all CSN sites based on season and NOAA climate region for the CMAQ531_WRF411_M3Dry_BiDi simulation.

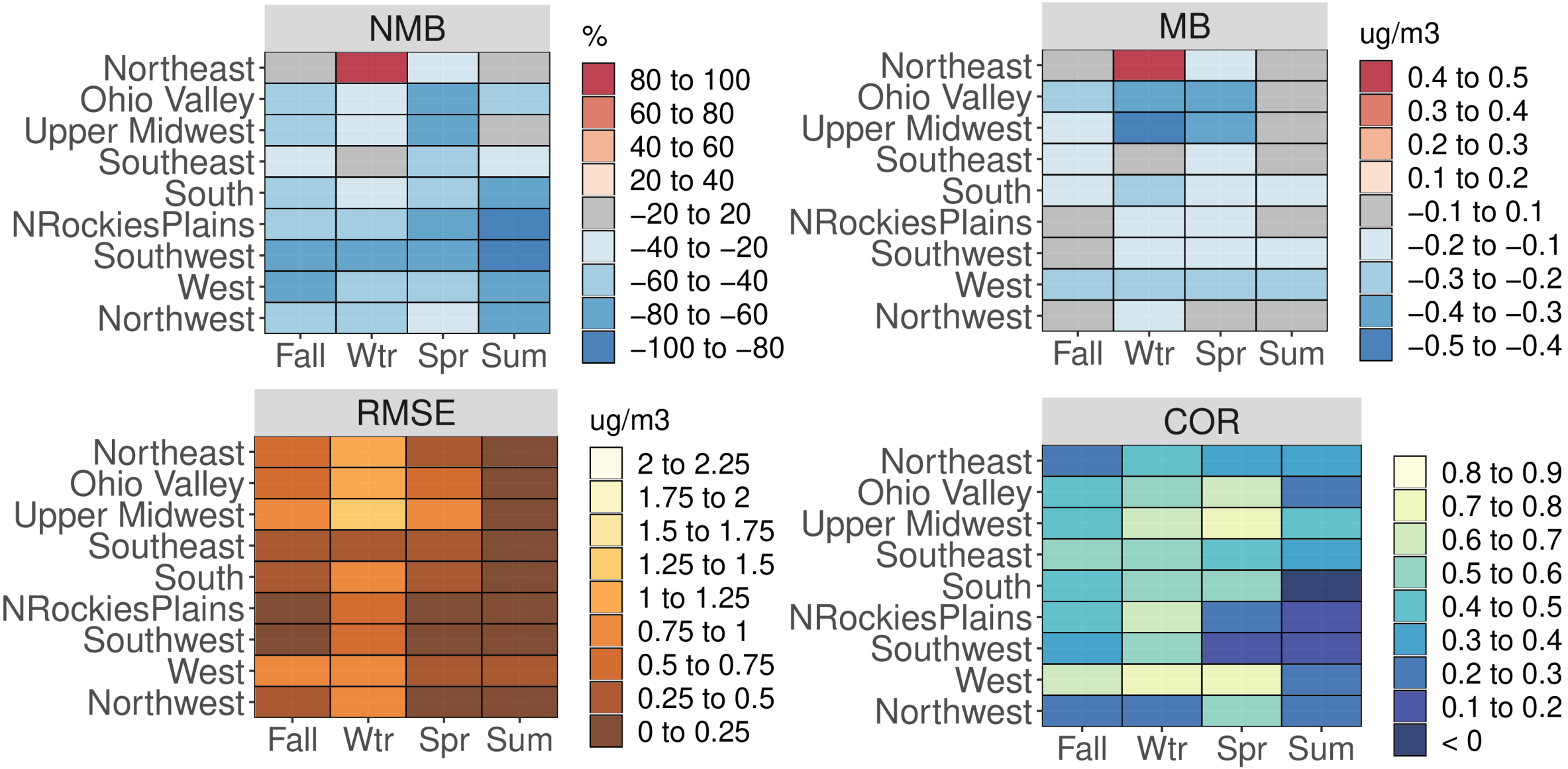

Figure S21. Categorical NMB (%), MB (μg m^{-3}), RMSE (μg m^{-3}), and Pearson correlation values for NO_3^- for all IMPROVE sites based on season and NOAA climate region for the CMAQ531_WRF411_M3Dry_BiDi simulation.

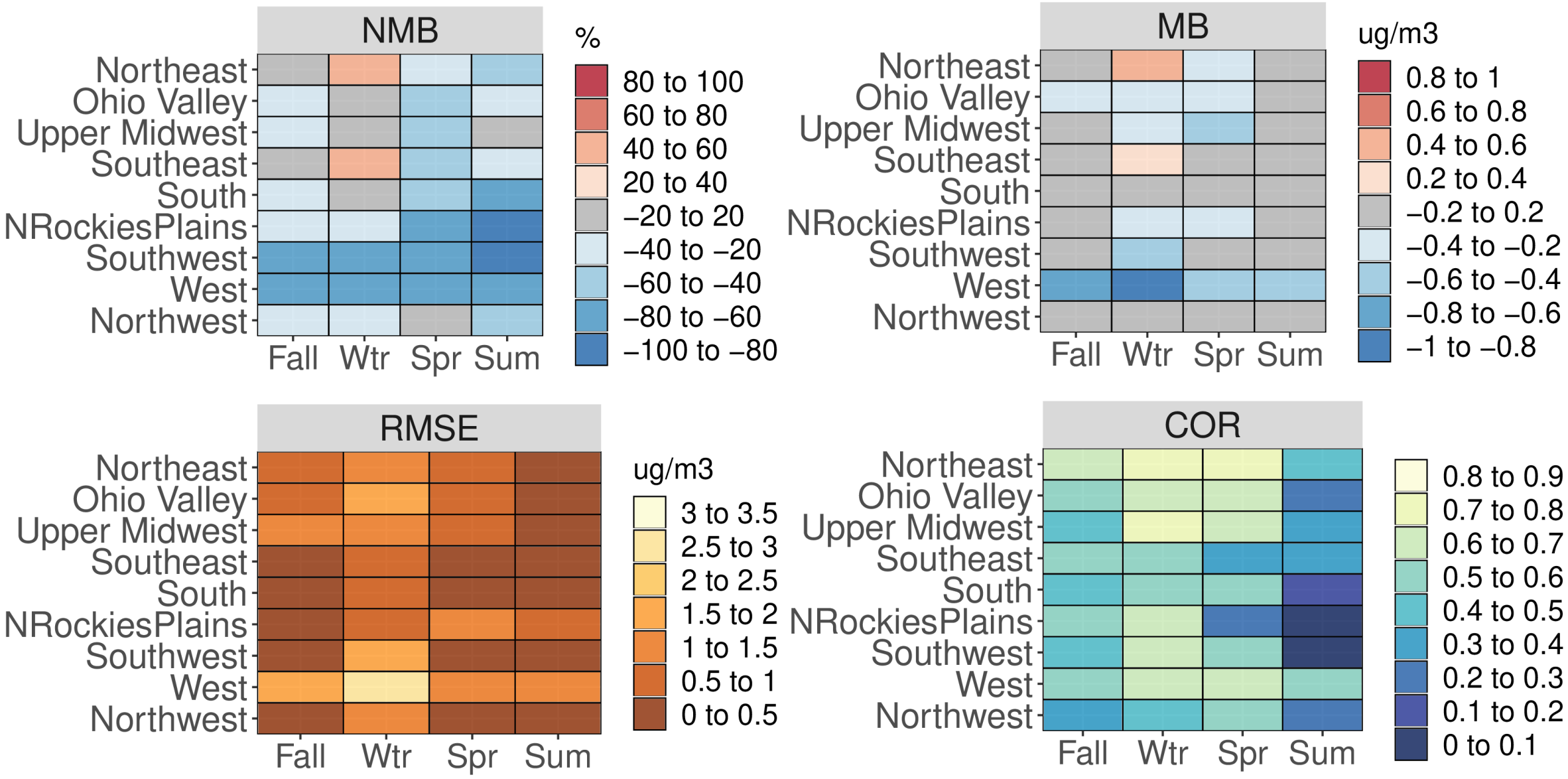

Figure S22. Categorical NMB (%), MB (μg m^{-3}), RMSE (μg m^{-3}), and Pearson correlation values for NO_3^- for all AQS sites based on season and NOAA climate region for the CMAQ531_WRF411_M3Dry_BiDi simulation.

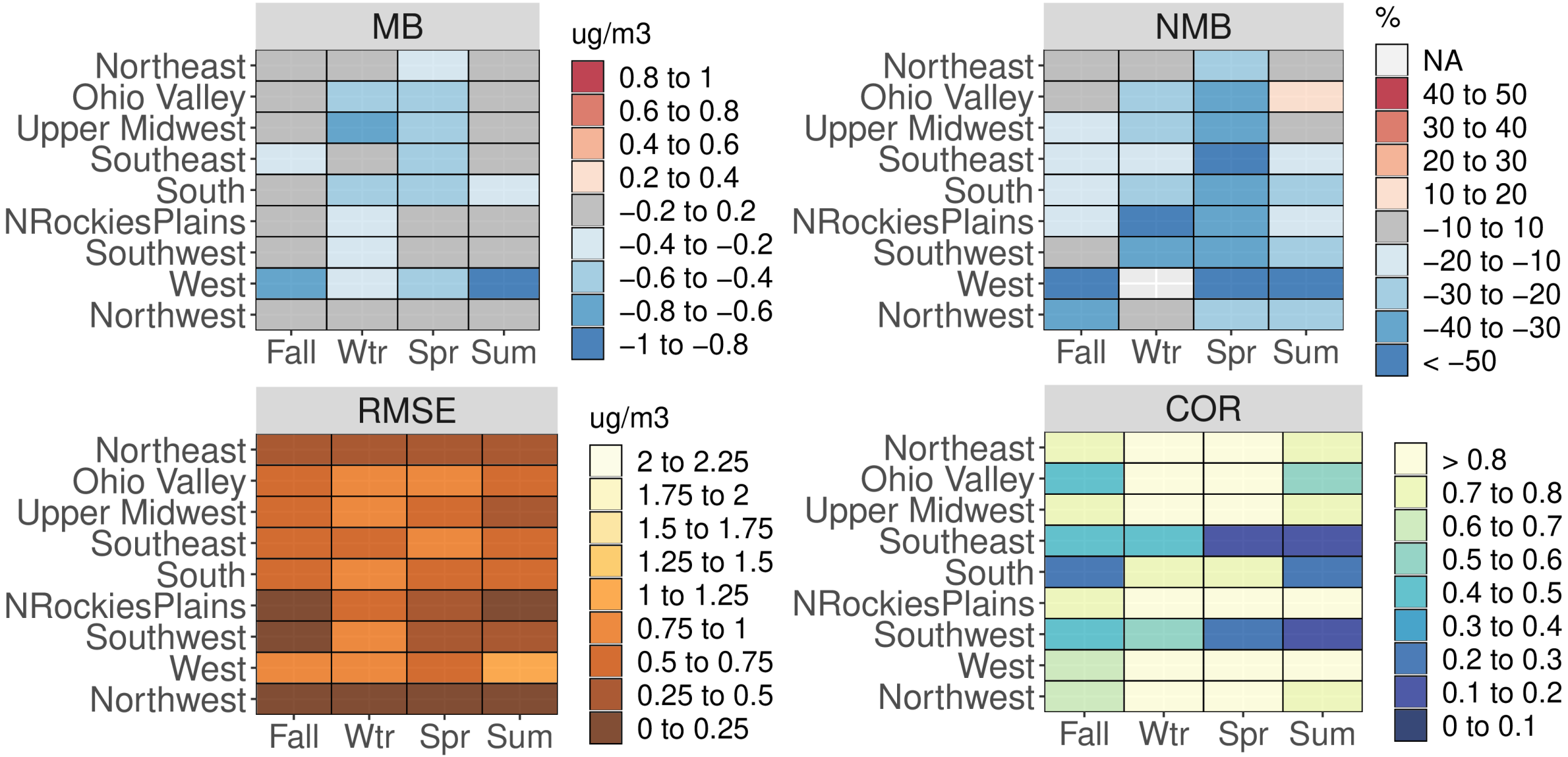

Figure S23. Categorical NMB (%), MB (μg m^{-3}), RMSE (μg m^{-3}), and Pearson correlation values for TNO_3^- for all CASTNet sites based on season and NOAA climate region for the CMAQ531_WRF411_M3Dry_BiDi simulation.

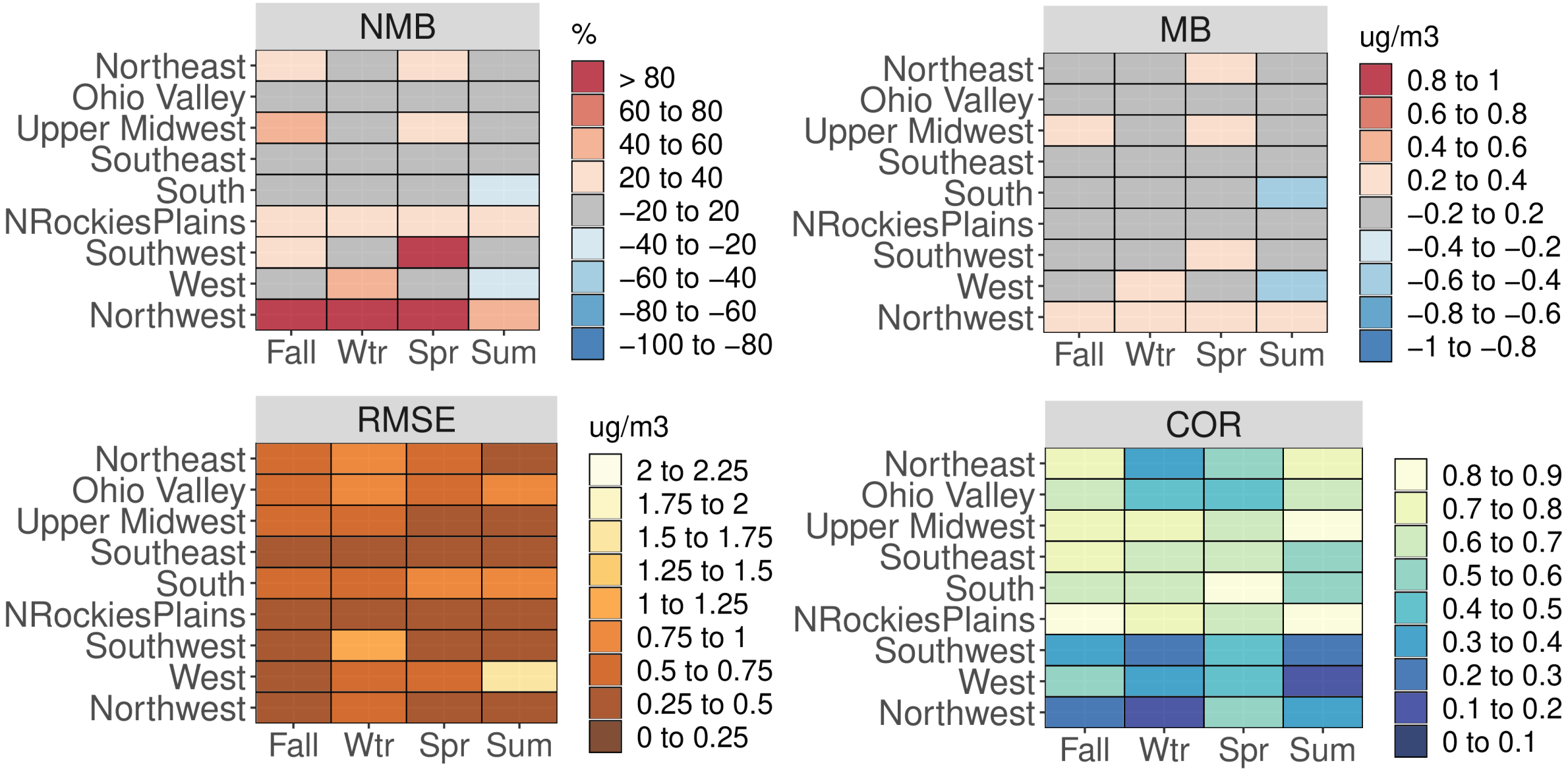

Figure S24. Categorical NMB (%), MB (μg m^{-3}), RMSE (μg m^{-3}), and Pearson correlation values for SO_4^{2-} for all CSN sites based on season and NOAA climate region for the CMAQ531_WRF411_M3Dry_BiDi simulation.

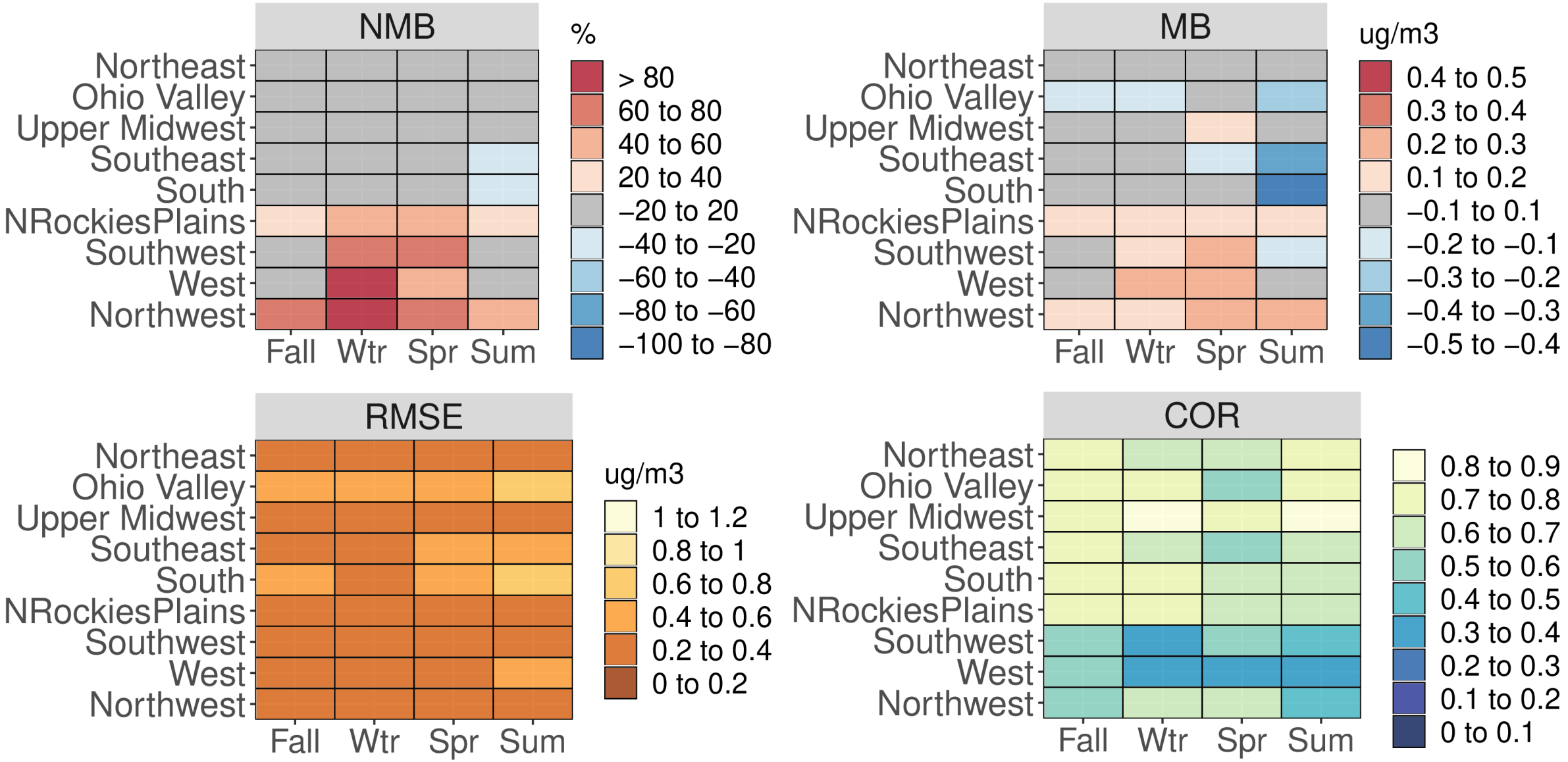

Figure S25. Categorical NMB (%), MB (μg m^{-3}), RMSE (μg m^{-3}), and Pearson correlation values for SO_4^{2-} for all IMPROVE sites based on season and NOAA climate region for the CMAQ531_WRF411_M3Dry_BiDi simulation.

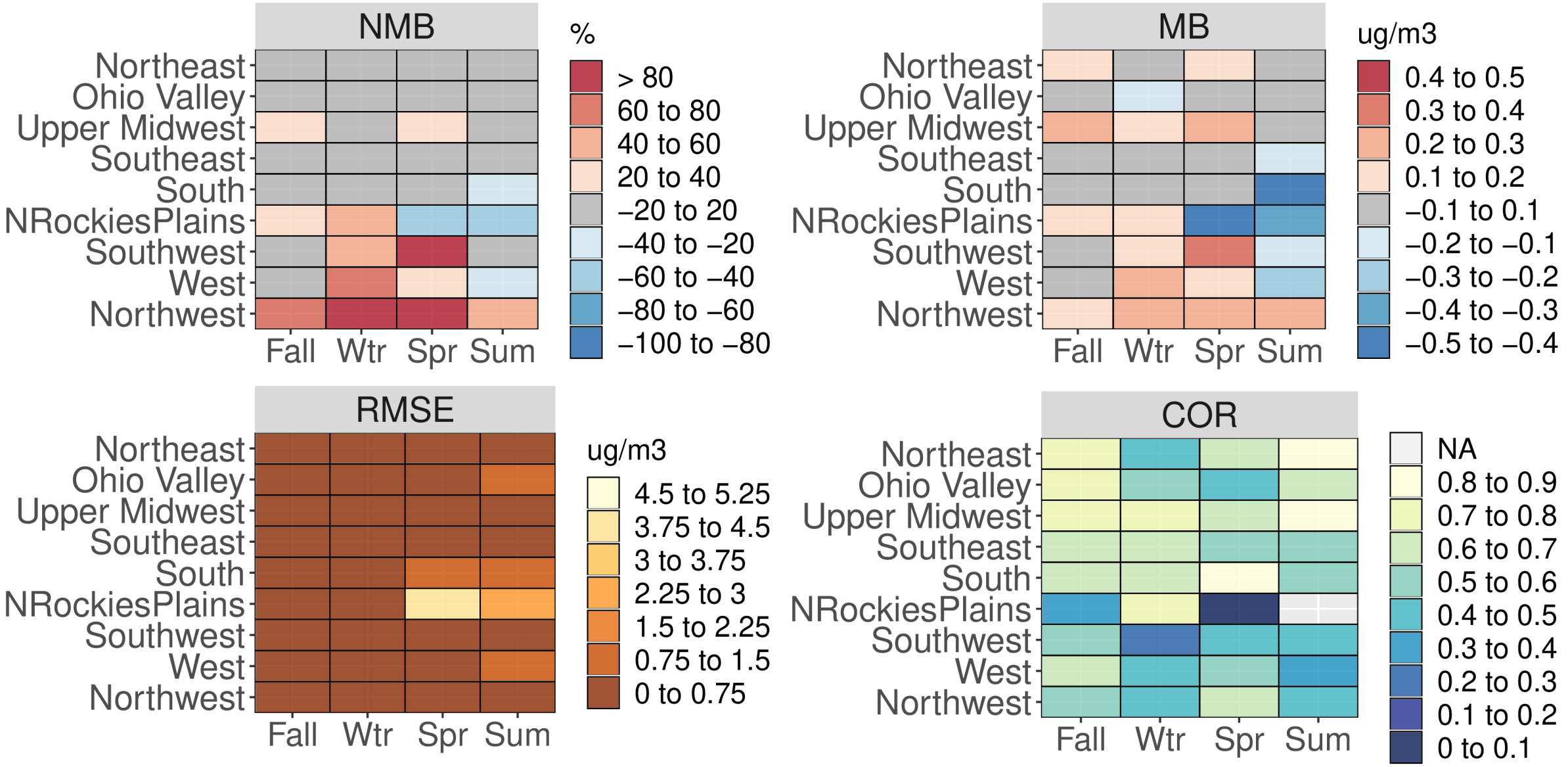

Figure S26. Categorical NMB (%), MB (μg m^{-3}), RMSE (μg m^{-3}), and Pearson correlation values for SO_4^{2-} for all AQS sites based on season and NOAA climate region for the CMAQ531_WRF411_M3Dry_BiDi simulation.

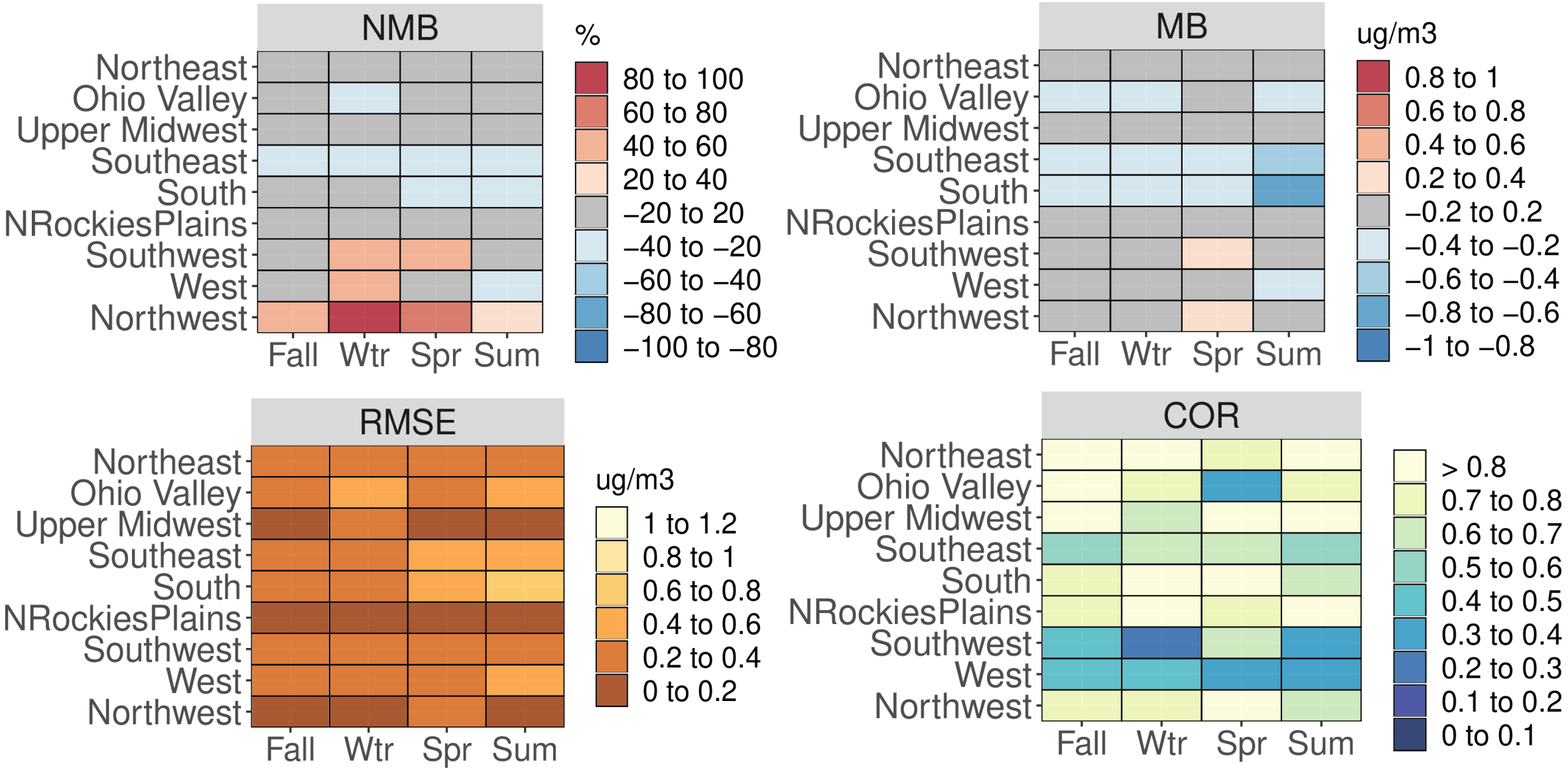

Figure S27. Categorical NMB (%), MB (μg m^{-3}), RMSE (μg m^{-3}), and Pearson correlation values for SO_4^{2-} for all CASTNet sites based on season and NOAA climate region for the CMAQ531_WRF411_M3Dry_BiDi simulation.

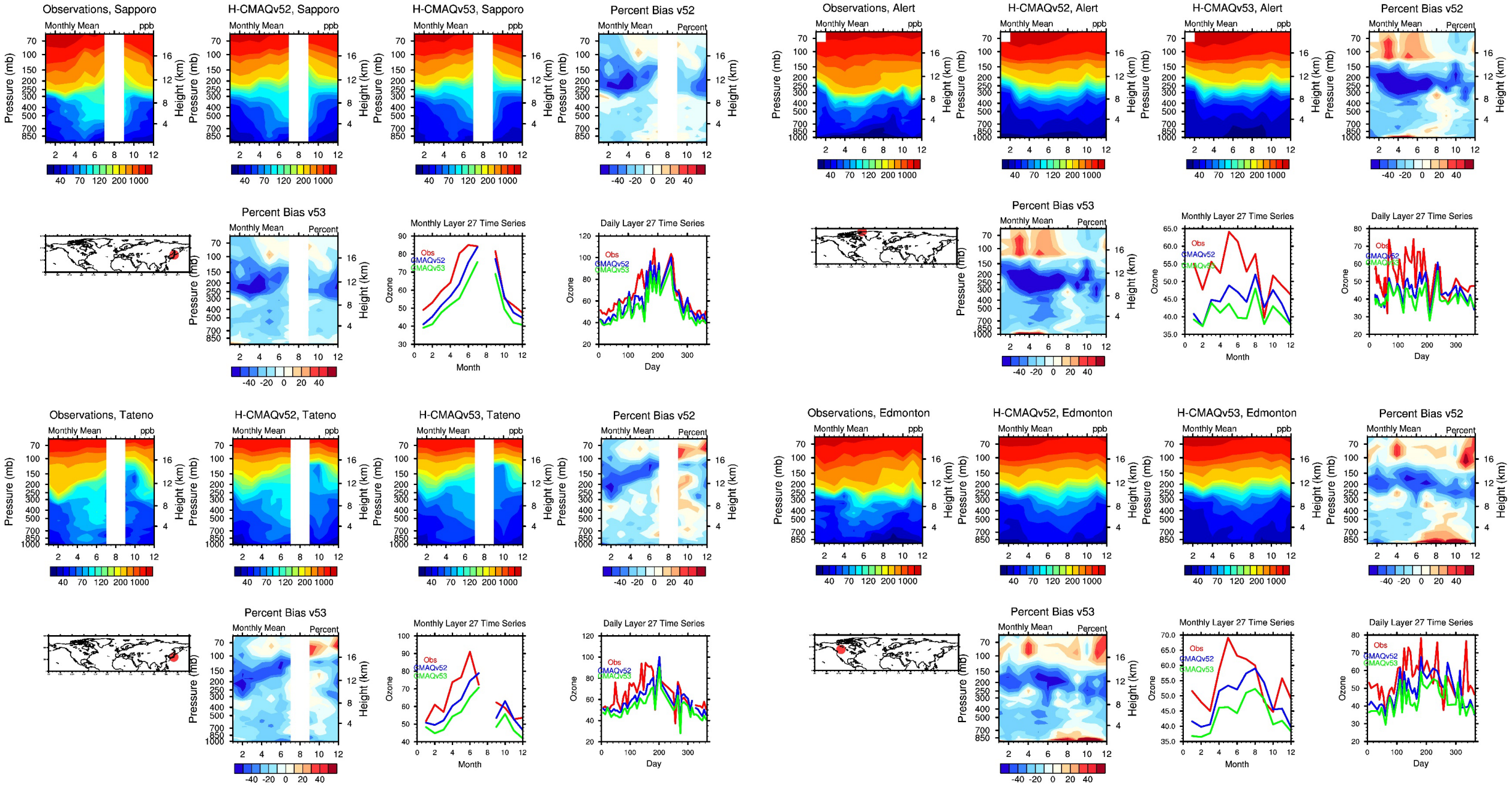

Figure S28. Comparison of ozonesonde data for the Sapporo, JP (upper left), Alert, GRL (upper right), Tateno, JP (lower left), and Edmonton, CA (lower right) WOUDC sites. Each panel consists of eight plots: observed O_3 (ppbv; top far left); HCMAQ52 modeled O_3 (ppbv; top middle left); HCMAQ53 modeled O_3 (ppbv; top middle right); HCMAQ52 bias (%; top far right); approximate site location (bottom far left); HCMAQ53 bias (%; bottom middle left); layer 27 monthly average O_3 time series (ppbv; bottom middle right); layer 27 daily average O_3 time series (ppbv; bottom far right).

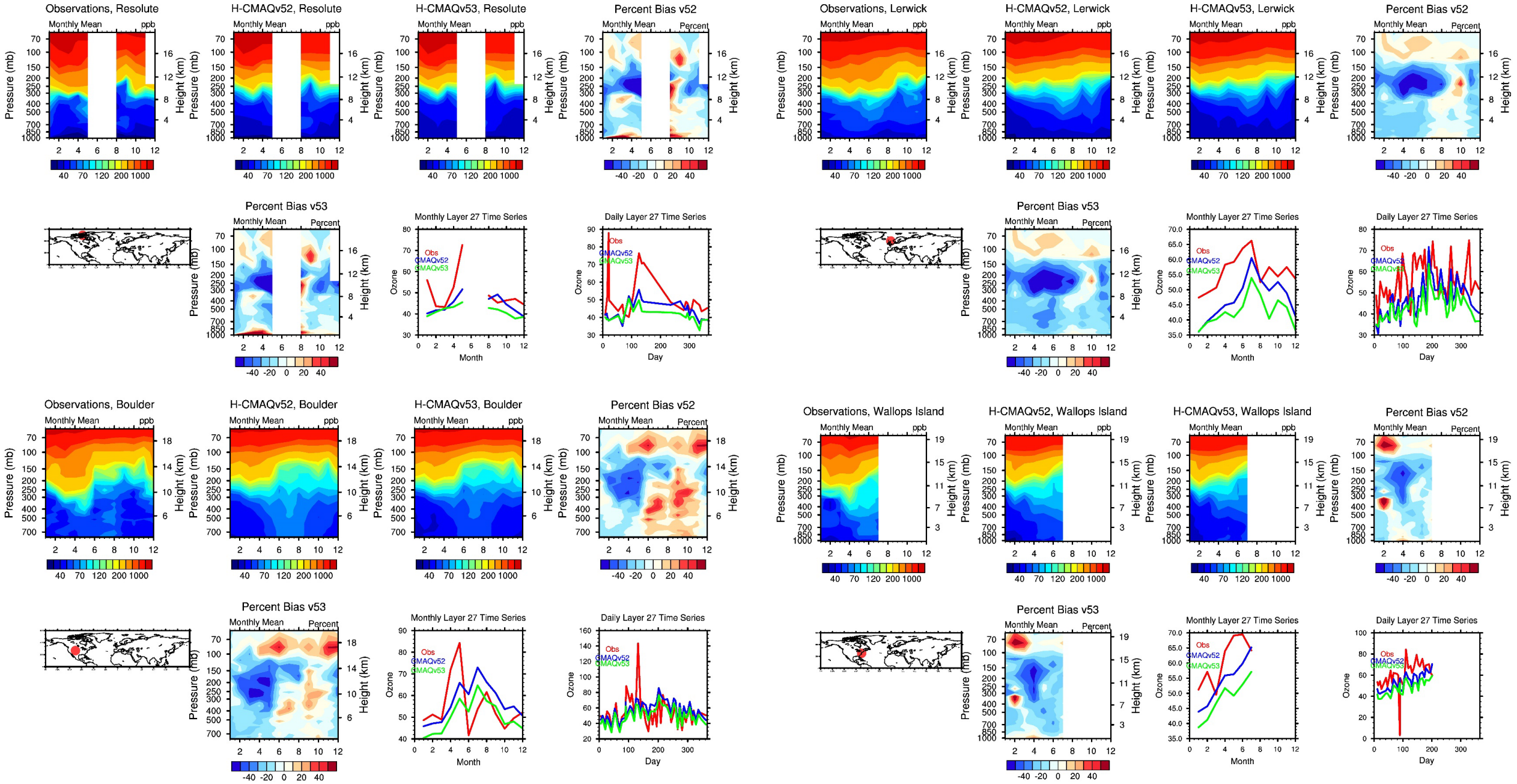

Figure S29. Comparison of ozonesonde data for the Resolute, CA (upper left), Lerwick, SCT (upper right), Boulder, US (lower left), and Wallops Island, US (lower right) WOUDC sites. Each panel consists of eight plots: observed O_3 (ppbv; top far left); HCMAQ52 modeled O_3 (ppbv; top middle left); HCMAQ53 modeled O_3 (ppbv; top middle right); HCMAQ52 bias (%; top far right); approximate site location (bottom far left); HCMAQ53 bias (%; bottom middle left); layer 27 monthly average O_3 time series (ppbv; bottom middle right); layer 27 daily average O_3 time series (ppbv; bottom far right).

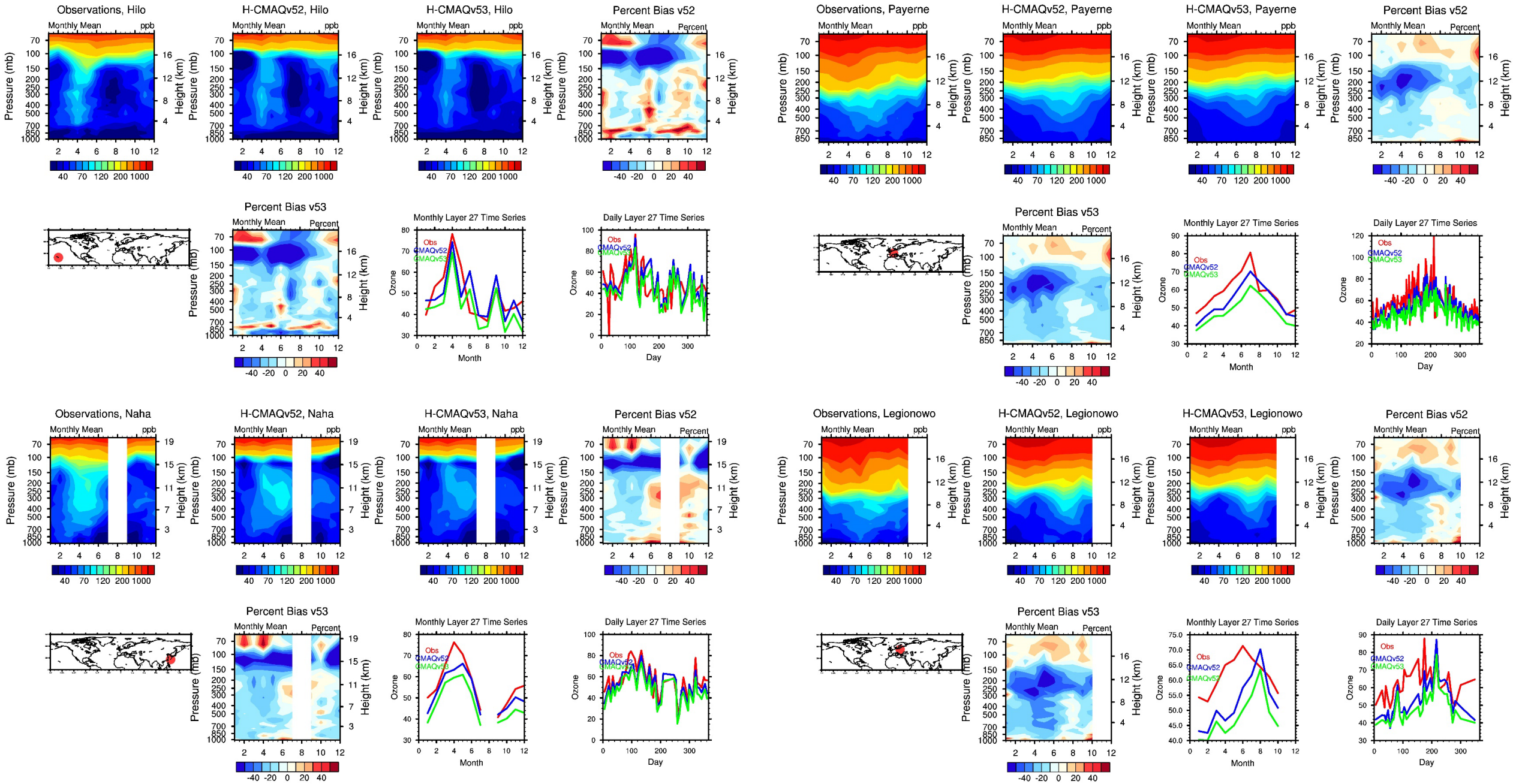

Figure S30. Comparison of ozonesonde data for the Hilo, US (upper left), Payerne, CH (upper right), Naha, JP (lower left), and Legionwo, PL (lower right) WOUDC sites. Each panel consists of eight plots: observed O_3 (ppbv; top far left); HCMAQ52 modeled O_3 (ppbv; top middle left); HCMAQ53 modeled O_3 (ppbv; top middle right); HCMAQ52 bias (%; top far right); approximate site location (bottom far left); HCMAQ53 bias (%; bottom middle left); layer 27 monthly average O_3 time series (ppbv; bottom middle right); layer 27 daily average O_3 time series (ppbv; bottom far right).

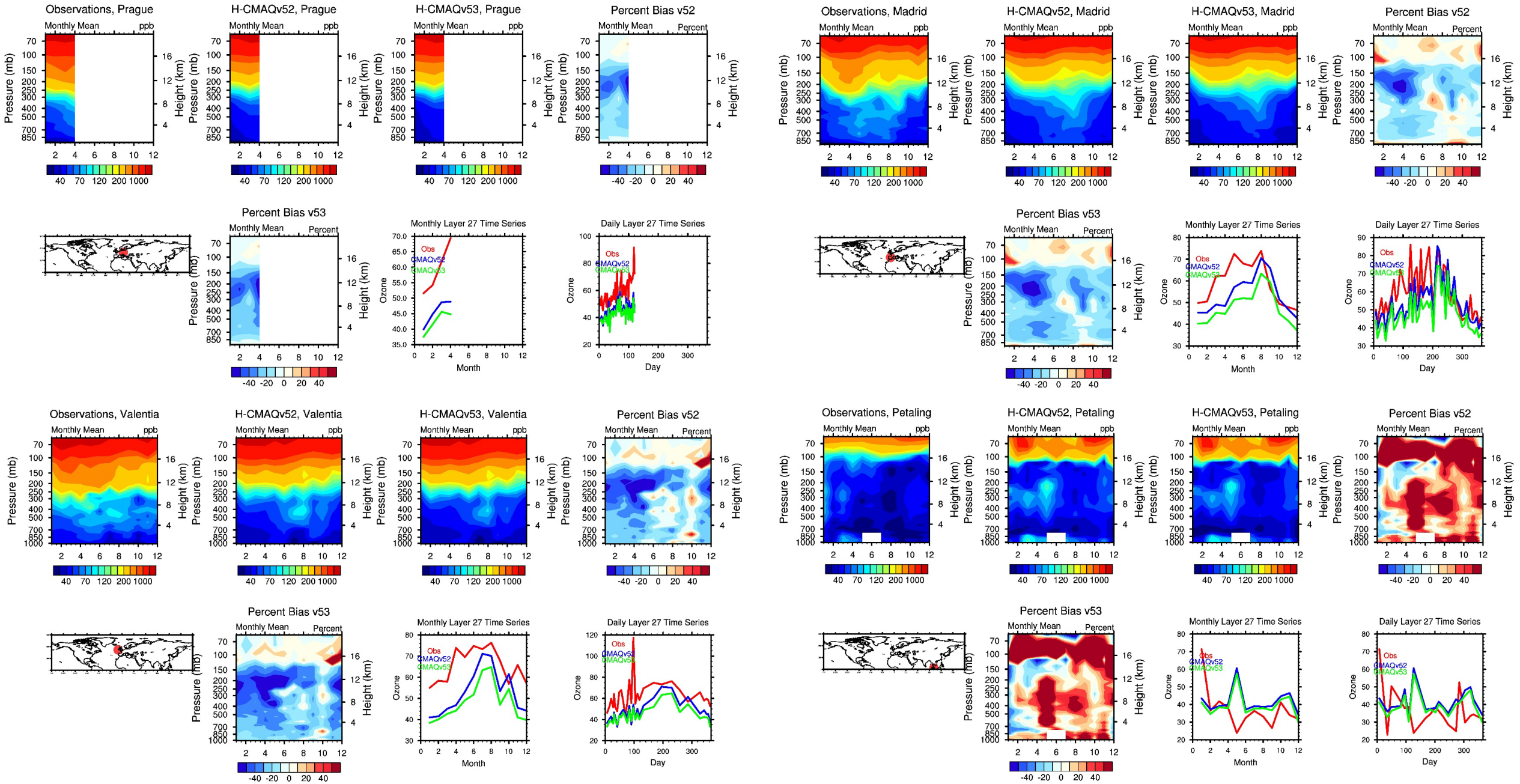

Figure S31. Comparison of ozonesonde data for the Prague, CZ (upper left), Mardrid, SP (upper right), Valentia, SP (lower left), and Petaling, MY (lower right) WOUDC sites. Each panel consists of eight plots: observed O_3 (ppbv; top far left); HCMAQ52 modeled O_3 (ppbv; top middle left); HCMAQ53 modeled O_3 (ppbv; top middle right); HCMAQ52 bias (%; top far right); approximate site location (bottom far left); HCMAQ53 bias (%; bottom middle left); layer 27 monthly average O_3 time series (ppbv; bottom middle right); layer 27 daily average O_3 time series (ppbv; bottom far right).

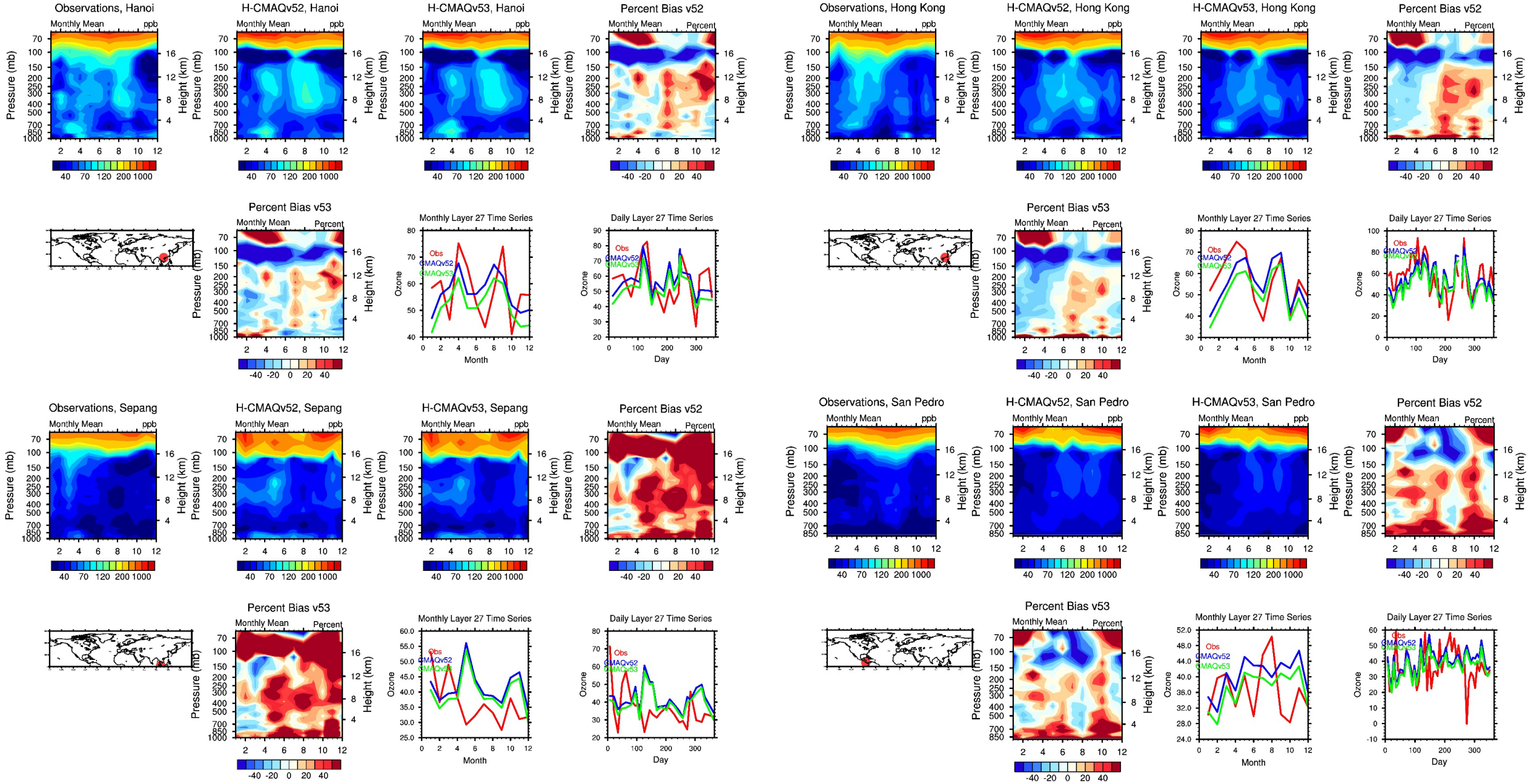

Figure S32. Comparison of ozonesonde data for the Hanoi, VT (upper left), Hong Kong, SAR (upper right), (lower left), and San Pedro, CR (lower right) WOUDC sites. Each panel consists of eight plots: observed O_3 (ppbv; top far left); HCMAQ52 modeled O_3 (ppbv; top middle left); HCMAQ53 modeled O_3 (ppbv; top middle right); HCMAQ52 bias (%; top far right); approximate site location (bottom far left); HCMAQ53 bias (%; bottom middle left); layer 27 monthly average O_3 time series (ppbv; bottom middle right); layer 27 daily average O_3 time series (ppbv; bottom far right).